

Study of SIDIS Unpolarized Cross Sections from a ^3He Target with the Solenoidal Large Intensity Device at JLab

Matteo Cerutti,^{1,2,3,*} Jian-Ping Chen,^{3,†} Umberto D'Alesio,^{4,‡} Haiyan Gao,^{5,6,§} Shuo Jia,^{5,6,¶} Vladimir Khachatryan,^{7,5,6,8,||} Alexei Prokudin,^{9,3,**} Lorenzo Rossi,^{10,††} Ye Tian,^{11,‡‡} and Zhiwen Zhao^{5,6,§§}

¹*IRFU, CEA, Université Paris-Saclay, F-91191 Gif-sur-Yvette, France*

²*Department of Physics, Christopher Newport University, Newport News, VA 23606, USA*

³*Jefferson Lab, Newport News, Virginia 23606, USA*

⁴*Università di Cagliari and INFN Sezione di Cagliari, I-09042 Monserrato (CA), Italy*

⁵*Physics Department, Duke University, Durham, NC 27708, USA*

⁶*Triangle Universities Nuclear Laboratory, Durham, NC 27708, USA*

⁷*Physics Department, Indiana University, Bloomington, IN 47405, USA*

⁸*Department of Physics and Astronomy, Mississippi State University, Starkville, MS 39762, USA*

⁹*Division of Science, Penn State University Berks, Reading, Pennsylvania 19610, USA*

¹⁰*Università degli Studi di Milano and INFN Sezione di Milano, I-20133 Milano, Italy*

¹¹*Department of Physics, Syracuse University, Syracuse, NY 13244, USA*

(Dated: December 25, 2025)

In this paper we present a detailed impact study of semi-inclusive deep inelastic scattering unpolarized cross sections' measurements using the proposed SoLID apparatus at Jefferson Lab. This type of data, collected at large Bjorken x_{bj} , moderate values of Q^2 and small values of the transverse momentum of produced hadrons, P_{hT} , allows to study transverse momentum dependent (TMD) parton distribution and fragmentation functions in a still poorly explored region. We present the projected results for charged light mesons based on simulated data. For the azimuthal-angle integrated cross sections we adopt the TMD framework up to the next-to-next-to-next-to-leading-logarithmic (N3LL) accuracy, while a simpler TMD parton model is employed for the study of azimuthal angular dependencies.

I. INTRODUCTION

A considerable amount of our knowledge about the quark-gluon composition of nucleons comes from intensive and detailed experimental and theoretical studies of the parton distribution functions (PDFs) [1] and fragmentation functions (FFs) [2]. Their precise knowledge is essential for a better comprehension of Quantum Chromodynamics (QCD), the theory of strong interactions, and of the partonic structure of the nucleon and hadronization mechanism. Furthermore, a deep understanding of QCD is essential to search for new physics beyond the Standard Model.

For quarks collinear to the parent hadron, the cross section for the deep inelastic scattering (DIS) [3] process, can be written in terms of collinear PDFs. At the lowest order, these PDFs have a clear physical interpretation as probability densities for finding an unpolarized parton in a fast-moving unpolarized nucleon, carrying a light-cone momentum fraction x . The integrated FFs, in turn, de-

scribe the hadronization process, namely how quarks and gluons transform into color-neutral hadrons. These are, by definition, one-dimensional (1D) maps of the internal dynamics of nucleons in momentum space. Moreover, the PDFs depend on a resolution (factorization) scale, associated with the hard scale Q^2 (four-momentum transfer squared) of the respective lepton-nucleon scattering process. Thanks to more than fifty years of dedicated efforts in their theoretical and experimental investigations, those PDFs are known at a very high accuracy [4–6].

However, over more than two decades, the frontier of PDF exploration has been extended to the three-dimensional (3D) momentum space. Such a 3D framework has been worked out in detail for semi-inclusive deep inelastic scattering (SIDIS) of a lepton scattered off a nucleon, in which the leading hadron is also detected and its transverse momentum, P_{hT} , is measured [7, 12]. In order to describe such a process, in the small P_{hT} region, one has to necessarily include the parton (quark) intrinsic transverse momentum \mathbf{k}_\perp in the scattering picture. More precisely, the regime in which the process can be described using transverse momentum dependent (TMD) factorization theorem, see e.g. Ref. [10, 12], corresponds to $q_T^2 \simeq P_{hT}^2/z^2 \ll Q^2$, where z is the light-cone fraction of the fragmenting quark momentum carried by the produced hadron, q_T is the transverse momentum of the exchanged virtual boson in a frame where the two hadrons are collinear. In TMD factorization the SIDIS cross section is given in terms of convolution of TMD PDFs and TMD FFs [2, 9, 11–17]

Proper combinations of the lepton beam and nucleon

* matteo.cerutti@cea.fr

† jpchen@jlab.org

‡ umberto.dalesio@ca.infn.it

§ haiyan.gao@duke.edu

¶ shuo.jia@duke.edu

|| vlakhach@iu.edu

** prokudin@jlab.org

†† lorenzo.rossi3@unimi.it

‡‡ tianye8001@gmail.com

§§ zwzhao@jlab.org

target polarizations in SIDIS experiments give rise to azimuthal modulations that include pivotal information on various TMDs [12]. These eventually allow us to quantify the quark transverse motion inside the nucleon, observe spin-spin and spin-orbit correlations, as well as obtain quantitative insight on the quark orbital angular momentum (OAM) [18]. It is important to stress that in order to access TMDs and have a complete 3D picture of the nucleon and of the fragmentation mechanism, measurements from different processes are essential: that is SIDIS from HERMES, COMPASS and JLab experiments [19–22], together with other processes such as Drell-Yan [23–25] and e^+e^- annihilation [2, 8, 26].

The SoLID Collaboration has meticulously designed and developed the concept of a large acceptance spectrometer (detector system) capable of handling high luminosities [27–29]. The proposed rich and vibrant SoLID science program will take advantage of the full potential of the JLab 12 GeV energy upgrade [30, 31]. There will be a new kinematic window for accomplishing precision studies of the transverse spin and TMD structure in the valence quark region for both neutron and proton. The experimental program on TMDs is considered one of the main pillars of the 12 GeV physics era at JLab.

The SIDIS part of the SoLID program includes three experiments on azimuthal single- and double-target spin asymmetry measurements, using transversely (E12-10-006 [32, 33]) and longitudinally (E12-11-007 [34]) polarized ^3He (as effective polarized neutron) targets, as well as a transversely (E12-11-108 [35]) polarized NH_3 (proton) target. To extract TMDs with high precision from these azimuthal asymmetry measurements, the detection system of SoLID will have a capability for handling large luminosities, a full (2π) azimuthal angular coverage, good kinematic coverage in terms of x_{b_j} (the Bjorken x), Q^2 (the virtuality of the exchanged photon), P_{hT} (the transverse momentum of the detected hadron), z_h (the scaling energy fraction of the produced hadron), and good PIDs (particle identification) for electrons and charged pions. Such a setup will allow for measurements in multi-dimensional (4D) kinematic bins with high statistics and well-controlled systematics.

Although azimuthal asymmetries provide information on spin-independent and spin-dependent TMD effects, mainly differential hadron multiplicity distributions (ratios between SIDIS and DIS cross sections) have been widely used in state-of-the-art extractions of unpolarized TMDs [36–39]. In contrast, there are limited studies on SIDIS unpolarized (and polarized) cross sections by themselves. Currently, the only available measurements of multiplicities are those from HERMES and COMPASS Collaborations [40–42]. While these measurements enabled such pioneering investigations, to study both the shape and the magnitude of the SIDIS cross sections and ascertain the validity of the factorization theorems, the information from absolute cross-section measurements is mandatory. The main reason is that while multiplicities, being *ratios* of differential cross sections, are cer-

tainly better under control from the experimental point of view (cancellation of systematics, etc.), they present some drawbacks from the theoretical point view, which can be summarized as follows: (*i*) the denominator of a multiplicity is an inclusive quantity, namely the inclusive DIS cross section, summed over all final-state hadrons, integrated over their kinematical variables and given in terms of ordinary structure functions, nevertheless, its numerator is less inclusive and strongly dependent on the kinematical cuts; (*ii*) these two factors entering the multiplicity are computed in different factorization schemes: its denominator in the collinear approach, while the numerator within a TMD approach; (*iii*) the assumptions and the approximations adopted in these two schemes (like the role played by higher-twist contributions in the numerator) are somehow different and independent. In other words, by integrating the numerator entering the multiplicity over all final-state hadronic variables (and summing over all hadrons), one does not necessarily recover its denominator.

All of this eventually implies that any discrepancy between experimental data and theoretical estimates can be ascribed to different issues, which are not straightforward to disentangle, including also what has been used for the denominator. This might be one of the reasons of the normalization problems encountered in past analyses [37, 38, 43]. In contrast, a direct comparison of absolute cross-section data with estimates obtained within a TMD factorization scheme allows for a direct and unbiased access to the non-perturbative parts of the TMDs (as the main goal), as well as for a test of certain assumptions adopted in this scheme and/or of the potential role of higher-twist contributions.

Since the SoLID projections we are going to show are obtained for a ^3He target, a comment on potential nuclear effects is mandatory. In this respect, currently their proper and consistent implementation within a TMD factorization approach is not yet fully developed (see Ref. [44] for pioneering studies). This is the main reason why, in the following, we adopt a simple model (in Sec. II C) based on isospin symmetry, without including any dilution factor. On the other hand, by using measurements of absolute cross sections off ^3He , Deuterium and Hydrogen targets, one will be able to extract important information on this factor. This could be eventually used for an estimate of nuclear effects and their role *posteriorly*, or complementarily, to tune current theoretical estimates and learn, at least indirectly, on nuclear TMDs. Notice that, once again, the role played by the measurements of absolute cross sections is fundamental in this respect. The use of multiplicities, as stressed above, in such a case would prevent any direct and unambiguous access to nuclear corrections, since many effects could mix up. Thereby, cross-section measurements will allow us to study many other effects that are usually neglected when working with multiplicities, such as nuclear corrections (EMC effect, nuclear binding, Fermi motion, off-shell effects), kinematic corrections, higher-twist effects,

and so on (see e.g. Ref. [45] and references therein). Notably, the unpolarized SIDIS cross section has already started to attract considerable interest almost a decade ago [46].

The first measurements of the unpolarized cross section is about measuring a large set of SIDIS cross sections in Hall C at JLab by the experiment E00-108 reported in [47, 48]. The measurements have been conducted for semi-inclusive charged-pion electro-production off proton and deuterium targets using a 5.5 GeV electron beam. Afterwards, a new measurement reported in [49, 50] has been carried out by the SIDIS experiment E06-010 in Hall A at JLab, using a 5.9 GeV polarized electron beam and a transversely polarized ^3He target. The upgraded beam energy experiment E12-09-017 (in Hall C), utilizing an 11 GeV longitudinally polarized electron beam scattered off proton and deuterium targets aims to determine the transverse momentum dependence of the SIDIS cross section [51] with results forthcoming.

The work in [49, 50] presents the current world data on the SIDIS unpolarized cross section, in multi-dimensional bin sets, compared with three theoretical models from [15, 52, 53], whereas the target ^3He nucleus is approximated as one neutron and two protons in a plane-wave scenario. Azimuthal modulations in that analysis were observed to be consistent with zero within the experimental uncertainties. Using a particular functional form, within a simplified leading-order (LO) TMD approach, as in the global analysis of Ref. [15], the fitted results showed that the width of the quark intrinsic transverse momentum, $\langle k_{\perp}^2 \rangle$, turned out to be much smaller than that determined from the global analyses of other types of data [15, 52–54]. Despite the general agreement between this simple model at the leading twist used in the analysis and the measured data, fairly large differences exist in some kinematic ranges, which might be related to higher-twist terms. Those terms might also be responsible for the very different $\langle k_{\perp}^2 \rangle$ values determined between that study and those from Refs. [15, 52–54]. In this respect, high-precision cross-section data in the moderate Q^2 range with a full azimuthal angular coverage (such as SoLID) can provide opportunities for exploring the higher-twist effects on azimuthal angular modulations, thereby significantly advancing our understanding of TMD physics. It is important to emphasize that theoretical proofs of factorization theorems exist for leading-twist observables, such as unpolarized SIDIS cross sections. Twist-3 observables are currently less studied theoretically, even though certain progress in next-to-leading power factorization has been achieved [55–59].

In this paper, we present a detailed analysis on the SIDIS unpolarized cross section measurements with the SoLID apparatus. In order to obtain physics-impact results with SoLID projections, we utilize a well-consolidated MAPTMD24 framework [38] with TMD evolution up to next-to-next-to-next-to-leading-logarithmic (N^3LL) accuracy. On the other hand, in the study of

the azimuthal modulations we will employ a simple, phenomenological LO TMD (or, generalized parton) model of Ref. [15]. Within this approach, TMDs will be parameterized starting from collinear distributions and assuming a transverse momentum dependence modeled as Gaussians. Although this approach is certainly too simple for the description of the actual experimental data, we believe that it can be very useful in exploring several issues. Studies on a variety of topics could originate when new data on the unpolarized cross section became available. Those may include analyses of nuclear effects in the large- x region, and higher-twist corrections (still unexplored theoretically). For the present unpolarized cross-section studies we project the simulated SoLID pseudo-data (including the statistical and systematic uncertainties) in various combinations of multi-dimensional bins of up to five variables – x_{bj} , P_{hT} , z_h , Q^2 , ϕ_h .

The paper is organized as follows. In Sec. II we describe the theoretical formalism, which underlies the generation of pseudo-data obtained from a modification of the original SIDIS event generator from [60]. Here we will pay great attention to the azimuthal-integrated and azimuthal-dependent cross-section scenarios. In Sec. III we discuss some results obtained from the implementation of nuclear effects (from Fermi motion) in the event generator. In Sec. IV and three appendices of this paper, we present the MAPTMD24+SoLID impact results both for the azimuthal-integrated and the azimuthal-dependent cross sections. Finally, we discuss our findings in Sec. V.

More details can be found in the approved proposal of Ref. [61], the proposed experiment of which will run parasitically to the SoLID SIDIS experiments E12-10-006 [32] and E12-11-007 [34].

II. SIDIS UNPOLARIZED CROSS SECTION: THEORETICAL FORMALISM

Here we present two complementary formalisms: one for the azimuthal-integrated cross sections and another one for their azimuthal angular dependencies. Due to the existing theoretical developments, we have to consider them separately and with different limitations/assumptions.

A. Basics of the general formalism

We consider the unpolarized SIDIS process in the γ^* - N center-of-mass frame, where the virtual photon moves along the positive z direction. The SIDIS process is represented as [12, 15–17, 62]

$$l(\ell) + N(P) \rightarrow l'(\ell') + h(P_h) + X, \quad (1)$$

where l is the incident lepton, N the target nucleon, l' the scattered lepton, and h the produced (final-state) hadron. The corresponding four-momenta are shown in parentheses. In this scattering process, the nucleon and

hadron masses are given by M_N and M_h , respectively. The cross section of the process is expressed in terms of the following invariants:

$$x_{bj} = \frac{Q^2}{2P \cdot q}, \quad y = \frac{P \cdot q}{P \cdot \ell}, \quad z_h = \frac{P \cdot P_h}{P \cdot q}, \quad \gamma = \frac{2M_N x_{bj}}{Q}, \quad (2)$$

with $q \equiv \ell - \ell'$ and the hard scale $Q^2 = -q^2$ describing the virtuality of the exchanged photon. The transverse momentum of the produced hadron is designated as $P_{hT} = |\mathbf{P}_{hT}|$, as shown in Fig. 1, where ϕ_h is the angle between the hadron production plane and the lepton scattering plane, while ϕ_S is the angle between the polarization vector of the target's spin and the lepton scattering plane. Notice that when not specified otherwise, by a_T or a_\perp , we always refer to the modulus of the corresponding vector.

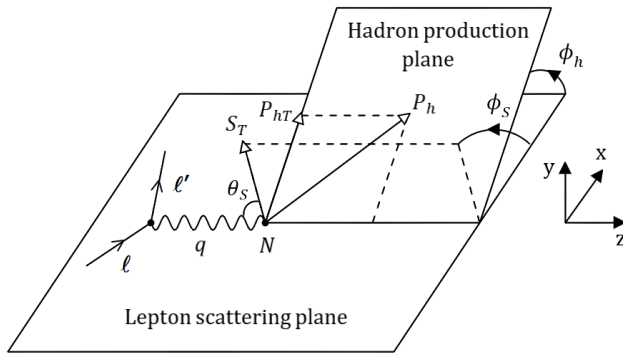


FIG. 1. Kinematics of the SIDIS process in Eq. (1), represented in the one-photon exchange approximation. The sketch follows the Trento conventions [62]. The x - z plane is defined by the initial ℓ and scattered ℓ' lepton momenta. The azimuthal angle ϕ_h is given in the target rest frame. The figure is taken from Ref. [63].

In the one-photon exchange approximation, the SIDIS unpolarized differential cross section is given by [12, 15, 49]

$$\frac{d\sigma}{dx_{bj} dz_h dQ dP_{hT}^2 d\phi_h} = \frac{4\pi\alpha^2}{x_{bj} Q^3} \left(1 + \frac{\gamma^2}{2x_{bj}}\right) \left[c_1 F_{UU} + c_2 \cos(\phi_h) F_{UU}^{\cos(\phi_h)} + c_3 \cos(2\phi_h) F_{UU}^{\cos(2\phi_h)} \right]. \quad (3)$$

In Eq. (3), α is the electromagnetic fine-structure constant; the coefficients c_1 , c_2 , and c_3 (see Eqs. (2.9)-(2.13)

of Ref. [12] for more details) are given by

$$c_1 = \frac{y^2}{2(1-\varepsilon)}, \quad c_2 = \frac{y^2}{2(1-\varepsilon)} \sqrt{2\varepsilon(1+\varepsilon)}, \quad c_3 = \frac{y^2}{2(1-\varepsilon)} \varepsilon, \quad (4)$$

where ε is the ratio of longitudinal and transverse photon fluxes:

$$\varepsilon = \frac{1 - y - (\gamma^2 y^2 / 4)}{1 - y + (y^2 / 2) + (\gamma^2 y^2 / 4)}. \quad (5)$$

The structure functions F_{UU} , $F_{UU}^{\cos(\phi_h)}$, and $F_{UU}^{\cos(2\phi_h)}$, depend on the kinematic variables x_{bj} , z_h , Q^2 , and P_{hT}^2 . F_{UU} survives upon integration over ϕ_h , while $F_{UU}^{\cos(\phi_h)}$ and $F_{UU}^{\cos(2\phi_h)}$ are structure functions related to the azimuthal $\cos(\phi_h)$ and $\cos(2\phi_h)$ modulations, respectively.

As mentioned previously, we will discuss F_{UU} by adopting the TMD factorization theorem and its phenomenological application at the current highest accuracy (Sec. II B), whereas $F_{UU}^{\cos(\phi_h)}$ and $F_{UU}^{\cos(2\phi_h)}$ will be studied at the parton model accuracy (Sec. II C).

B. Azimuthal-integrated cross sections

Here we discuss the structure function F_{UU} , adopting the TMD factorization theorem within the Collins-Soper-Sterman (CSS) framework [64, 65]. We will give only the main formulas relevant for the analysis we are interested in. All the details can be found in the literature (see, for instance, Ref. [38], where the advanced MAPTMD24 framework by the MAP Collaboration is presented).

A word of caution is needed on the definition of transverse momenta. Indeed, we consider the transverse component of the produced hadron momentum with respect to P , and q (P_{hT}) or, equivalently, the transverse component ($q_T = |\mathbf{q}_T|$) of the virtual photon momentum with respect to P and P_h (in a frame, where these momenta are collinear). These are related as follows:

$$q_T^2 \sim P_{hT}^2 / z_h^2. \quad (6)$$

The unpolarized cross section at small transverse momenta, integrated over the azimuthal angle ϕ_h and neglecting the target mass, can be expressed as

$$\frac{d\sigma^{\text{SIDIS}}}{dx_{bj} dz_h dq_T dQ} = \frac{8\pi^2 \alpha^2 z_h^2 q_T}{x_{bj} Q^3} \times \left[1 + \left(1 - \frac{Q^2}{x_{bj} s}\right)^2 \right] F_{UU}(x_{bj}, z_h, q_T, Q^2),$$

$$\begin{aligned}
F_{UU}(x_{bj}, z_h, q_T, Q^2) &= x_{bj} \mathcal{H}^{\text{SIDIS}}(Q, \mu) \sum_a e_a^2 \\
&\times \int d^2 \mathbf{k}_\perp \int \frac{d^2 \mathbf{P}_\perp}{z^2} f_1^a(x, \mathbf{k}_\perp^2; \mu, \zeta_A) D_1^{a \rightarrow h}(z, \mathbf{P}_\perp^2; \mu, \zeta_B) \delta^{(2)}(\mathbf{k}_\perp + \mathbf{P}_\perp/z + \mathbf{q}_T), \quad (7)
\end{aligned}$$

where the sum in F_{UU} runs over all active quark flavors. The hard factor $\mathcal{H}^{\text{SIDIS}}$ is perturbatively computable and depends on Q and a renormalization scale μ . The last line contains the convolution of the unpolarized TMD PDF, f_1^a , as a function of the rapidity scale ζ_A and of the transverse momentum $k_\perp = |\mathbf{k}_\perp|$ of the struck quark with respect to the nucleon momentum, as well as the TMD FF, $D_1^{a \rightarrow h}$, as a function of the rapidity scale ζ_B and of the transverse momentum $P_\perp = |\mathbf{P}_\perp|$ of the produced hadron h with respect to the fragmenting quark axis. To have a better visualization, in Fig. 2 we show the involved transverse momenta in the γ^*-N center-of-mass frame. The struck parton, carrying the four-momentum $p = k + q$, fragments into a hadron with four-momentum P_h that has a transverse momentum P_\perp with respect to the fragmenting quark axis. The total (measured) transverse momentum of the final-state hadron is P_{hT} , and in the large- Q^2 limit $P_{hT} \approx zk_\perp + P_\perp$.

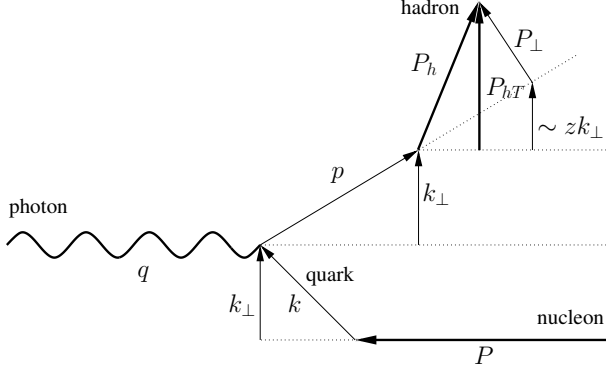


FIG. 2. Relevant SIDIS momenta in the γ^*-N center-of-mass frame: q is the virtual photon momentum, k is the momentum of the initial quark with transverse momentum k_\perp inside a nucleon with momentum P . The figure is taken from [38], where the photon line stands for a virtual photon.

In the following, we adopt the large- Q limit, where $x = x_{bj}$ and $z = z_h$. As usual, one works in the conjugate position space (\mathbf{b}_T space) by defining the Fourier transforms of the TMD PDF

$$\begin{aligned}
\hat{f}_1^a(x, \mathbf{b}_T^2; \mu, \zeta) &= \int d^2 \mathbf{k}_\perp e^{i\mathbf{b}_T \cdot \mathbf{k}_\perp} f_1^a(x, \mathbf{k}_\perp^2; \mu, \zeta) \\
&= 2\pi \int_0^\infty dk_\perp k_\perp J_0(b_T k_\perp) f_1^a(x, \mathbf{k}_\perp^2; \mu, \zeta), \quad (8)
\end{aligned}$$

and the TMD FF

$$\begin{aligned}
\hat{D}_1^{a \rightarrow h}(z, \mathbf{b}_T^2; \mu, \zeta) &= \\
&= \int \frac{d^2 \mathbf{P}_\perp}{z^2} e^{-i\mathbf{b}_T \cdot \mathbf{P}_\perp/z} D_1^a(z, \mathbf{P}_\perp^2; \mu, \zeta) \\
&= 2\pi \int_0^\infty \frac{dP_\perp}{z^2} P_\perp J_0(b_T P_\perp/z) D_1^a(z, \mathbf{P}_\perp^2; \mu, \zeta), \quad (9)
\end{aligned}$$

where J_0 is the Bessel function of the first kind. The convolution in the second line of Eq. (7) can be rewritten as

$$\begin{aligned}
&\frac{1}{2\pi} \int_0^{+\infty} db_T b_T J_0(b_T q_T) \times \\
&\times \hat{f}_1^a(x, \mathbf{b}_T^2; \mu, \zeta_A) \hat{D}_1^{a \rightarrow h}(z, \mathbf{b}_T^2; \mu, \zeta_B). \quad (10)
\end{aligned}$$

Focusing on the evolution of TMD PDFs (an analogous description applies to TMD FFs as well), i.e., the dependence on the renormalization scale μ and the rapidity scale ζ , the complete set of equations is given by

$$\begin{aligned}
\frac{\partial \ln \hat{f}_1(x, \mathbf{b}_T^2, \mu, \zeta)}{\partial \ln \mu} &= \gamma_F \left(\alpha_s(\mu), \frac{\zeta}{\mu^2} \right), \\
\frac{\partial \hat{f}_1(x, \mathbf{b}_T^2, \mu, \zeta)}{\partial \ln \sqrt{\zeta}} &= K(b_T, \mu), \\
\frac{\partial K(b_T, \mu)}{\partial \ln \mu} &= -\gamma_K(\alpha_s(\mu)), \quad (11)
\end{aligned}$$

where γ_F/K are the anomalous dimensions of the renormalization-group and of the Collins-Soper evolution equations, respectively, while γ_K is the so-called cusp anomalous dimension.

These differential equations allow us to determine TMD PDFs at any final pair of scales (μ_f, ζ_f) , starting from an initial pair (μ_i, ζ_i) . In addition, in the region of small b_T , the TMD PDF, \hat{f}_1 , is matched onto its corresponding collinear PDF, f_1 , through a convolution with suitable perturbative matching coefficients C . The resulting expression at the final scales (μ_f, ζ_f) is

$$\begin{aligned}
\hat{f}_1(x, \mathbf{b}_T^2; \mu_f, \zeta_f) &= [C \otimes f_1](x, \mathbf{b}_T^2; \mu_i, \zeta_i) \times \\
&\times \exp \left\{ K(\mu_i) \ln \left(\frac{\sqrt{\zeta_f}}{\sqrt{\zeta_i}} \right) + \right. \\
&\left. + \int_{\mu_i}^{\mu_f} \frac{d\mu}{\mu} \left[\gamma_F(\alpha_s(\mu), 1) - \gamma_K(\alpha_s(\mu)) \ln \left(\frac{\sqrt{\zeta_f}}{\mu} \right) \right] \right\}. \quad (12)
\end{aligned}$$

More details can be found in Ref. [38] and references therein.

The initial scale μ_i is commonly chosen for simplifying the calculations of perturbative ingredients. More

precisely, one adopts $\mu_i \sim 1/b_T$; this choice, while well under control at small b_T , manifests a problem when b_T becomes too large: the hitting of the Landau pole when computing the QCD coupling constant at too low μ_i . A suitable and well consolidated prescription to

cure this problem within the CSS framework is the so-called b_* -prescription, by redefining μ_i as $\mu_{b_*} \sim 1/b_*(b_T)$. Through this procedure, the TMD PDF in Eq. (12) can be written as

$$\hat{f}_1(x, \mathbf{b}_T^2; \mu_f, \zeta_f) = \hat{f}_1(x, \mathbf{b}_T^2; \mu_f, \zeta_f) \Big|_{\text{pert}} \hat{f}_{\text{NP}}(x, \mathbf{b}_T^2; \zeta, Q_0), \quad (13)$$

namely, in terms of the product between a fully perturbatively calculable expression and a nonperturbative function that must be fitted to experimental data (Q_0 is the scale at which this latter contribution is parametrized).

In this analysis we consider the parameterization of

\hat{f}_{NP} taken from the recent N³LL extraction of [38], where a detailed study of the flavor dependence was carried out at the currently available highest theoretical accuracy. For clarity, we report the MAPTMD24 model selected for the TMD PDF, \hat{f}_1 :

$$f_{\text{NP}}(x, \mathbf{b}_T^2; \zeta, Q_0) = \frac{g_1(x) e^{-g_1(x) \frac{\mathbf{b}_T^2}{4}} + \lambda^2 g_2^2(x) \left[1 - g_2(x) \frac{\mathbf{b}_T^2}{4} \right] e^{-g_2(x) \frac{\mathbf{b}_T^2}{4}} + \lambda_2^2 g_3(x) e^{-g_3(x) \frac{\mathbf{b}_T^2}{4}}}{g_1(x) + \lambda^2 g_2^2(x) + \lambda_2^2 g_3(x)} \left[\frac{\zeta}{Q_0^2} \right]^{g_K(\mathbf{b}_T^2)/2}, \quad (14)$$

corresponding to the Fourier transform of the sum of two

Gaussians and a Gaussian weighted by \mathbf{k}_\perp^2 . The analogous expression of the model for the TMD FF, \hat{D}_1 , is

$$D_{1\text{NP}}(z, \mathbf{b}_T^2; \zeta, Q_0) = \frac{g_4(z) e^{-g_4(z) \frac{\mathbf{b}_T^2}{4z^2}} + \frac{\lambda_F}{z^2} g_5^2(z) \left[1 - g_5(z) \frac{\mathbf{b}_T^2}{4z^2} \right] e^{-g_5(z) \frac{\mathbf{b}_T^2}{4z^2}}}{g_4(z) + \frac{\lambda_F}{z^2} g_5^2(z)} \left[\frac{\zeta}{Q_0^2} \right]^{g_K(\mathbf{b}_T^2)/2}, \quad (15)$$

corresponding to the Fourier transform of the sum of a Gaussian and a Gaussian weighted by \mathbf{P}_\perp^2 . The g_i functions represent the widths of the distributions and include a dependence on the variables x and z :

$$g_{\{1,2,3\}}(x) = N_{\{1,2,3\}} \frac{x^{\sigma_{\{1,2,3\}}} (1-x)^{\alpha_{\{1,2,3\}}^2}}{\hat{x}^{\sigma_{\{1,2,3\}}} (1-\hat{x})^{\alpha_{\{1,2,3\}}^2}}, \quad (16)$$

$$g_{\{4,5\}}(z) = N_{\{4,5\}} \frac{\left(z^{\beta_{\{1,2\}}} + \delta_{\{1,2\}}^2 \right) (1-z)^{\gamma_{\{1,2\}}^2}}{\left(\hat{z}^{\beta_{\{1,2\}}} + \delta_{\{1,2\}}^2 \right) (1-\hat{z})^{\gamma_{\{1,2\}}^2}}. \quad (17)$$

with $\hat{x} = 0.1$, $\hat{z} = 0.5$, and N_i (with $i = 1, 2, 3, 4, 5$), σ_j , α_j (with $j = 1, 2, 3$), β_i , δ_i , γ_i (with $i = 1, 2$), all being as free parameters. Finally, g_K is the non perturbative part of the Collins-Soper kernel: namely, the evolution on the rapidity scale ζ , and is parametrized as

$$g_K(\mathbf{b}_T^2) = -g_2^2 \frac{\mathbf{b}_T^2}{2}, \quad (18)$$

where we set $Q_0 = 1$ GeV.

The MAPTMD24 global fit, employed in this SIDIS unpolarized cross-section analysis, can be considered as the current state-of-the-art phenomenological extraction of TMD PDFs and TMD FFs. For completeness, we should mention that another simultaneous extraction of same quantities at the current best accuracy has appeared very recently in Ref. [39], namely the ART25 fit.

C. Azimuthal angular-dependent cross sections

We now move on to the discussion of the azimuthal dependence in the unpolarized cross section in Eq. (3). In such a case, we cannot utilize the full machinery discussed in the previous section. Nonetheless, even by adopting a simplified TMD framework, at a lower level of accuracy, we will be able to show what one can learn from this study, putting some bases for future improved analyses.

Thus, we will focus on $F_{UU}^{\cos(\phi_h)}$ and $F_{UU}^{\cos(2\phi_h)}$; besides,

for consistency and internal coherence, we will also discuss F_{UU} in the same framework. Hereinafter, we mainly follow Ref. [15], showing some of its formulas, which we use in this part of our analysis for calculating the central values of the unpolarized cross-section pseudo-data. Consistently, we will directly work in \mathbf{k}_\perp space.

The LO factorization scheme of Eq. (3), supplemented by Eq. (4), is equivalent to Eq. (3) of Ref. [15], with

$$F_{UU} = \sum_q e_q^2 x \int d^2 \mathbf{k}_\perp f_q(x, \mathbf{k}_\perp^2) D_q(z, \mathbf{P}_\perp^2), \quad (19)$$

where the sum is assumed to be over quarks and antiquarks. The Q^2 dependence of both functions in the

integrand is omitted for simplicity. This enters the azimuthal-independent part of Eq. (3) and it is the leading-order expression of the F_{UU} in Eq. (7), after applying the momentum conservation condition

$$\mathbf{P}_{hT} = z \mathbf{k}_\perp + \mathbf{P}_\perp. \quad (20)$$

The second structure function in Eq. (3), $F_{UU}^{\cos(\phi_h)}$, associated to the $\cos(\phi_h)$ modulation of the cross section, is a twist-3 quantity of the order of $1/Q$. It can be written as the sum of the Cahn and Boer-Mulders contributions:

$$F_{UU}^{\cos(\phi_h)} = F_{UU}^{\cos(\phi_h)}|_{\text{Cahn}} + F_{UU}^{\cos(\phi_h)}|_{\text{BM}}. \quad (21)$$

Herein we have

$$F_{UU}^{\cos(\phi_h)}|_{\text{Cahn}} = -2 \sum_q e_q^2 x \int d^2 \mathbf{k}_\perp \frac{(\mathbf{k}_\perp \cdot \hat{\mathbf{h}})}{Q} f_q(x, \mathbf{k}_\perp^2) D_q(z, \mathbf{P}_\perp^2), \quad (22)$$

$$F_{UU}^{\cos(\phi_h)}|_{\text{BM}} = \sum_q e_q^2 x \int d^2 \mathbf{k}_\perp \frac{k_\perp P_{hT} - z(\mathbf{k}_\perp \cdot \hat{\mathbf{h}})}{k_\perp} \Delta f_{q^\uparrow/p}(x, \mathbf{k}_\perp^2) \Delta D_{h/q^\uparrow}(z, \mathbf{P}_\perp^2), \quad (23)$$

where $\hat{\mathbf{h}} \equiv \mathbf{P}_{hT}/|\mathbf{P}_{hT}|$ is a unit vector. The Cahn contribution in Eq. (22) involves the convolution of $f_q(x, \mathbf{k}_\perp^2)$ and $D_q(z, \mathbf{P}_\perp^2)$. The Boer-Mulders contribution in Eq. (23) involves the convolution of the Boer-Mulders TMD $\Delta f_{q^\uparrow/p}(x, \mathbf{k}_\perp^2)$ and the Collins FF $\Delta D_{h/q^\uparrow}(z, \mathbf{P}_\perp^2)$. These two functions are in turn represented by the following expressions:

$$\Delta f_{q^\uparrow/p}(x, \mathbf{k}_\perp^2) = -\frac{k_\perp}{M_p} h_1^\perp(x, \mathbf{k}_\perp^2), \quad (24)$$

$$\Delta D_{h/q^\uparrow}(z, \mathbf{P}_\perp^2) = \frac{2P_\perp}{zM_h} H_1^\perp(z, \mathbf{P}_\perp^2), \quad (25)$$

according to the Amsterdam notation [12]. The function

h_1^\perp describes a quark's transverse polarization asymmetry inside an unpolarized nucleon [9]. The function H_1^\perp describes the asymmetric distribution in the fragmentation of a transversely polarized quark into an unpolarized hadron [66].

The third structure function in Eq. (3), $F_{UU}^{\cos(2\phi_h)}$, associated to the $\cos(2\phi_h)$ modulation of the cross section, consists of a twist-4 Cahn contribution and a twist-2 Boer-Mulders term:

$$F_{UU}^{\cos(2\phi_h)} \approx F_{UU}^{\cos(2\phi_h)}|_{\text{Cahn}} + F_{UU}^{\cos(2\phi_h)}|_{\text{BM}}, \quad (26)$$

where

$$F_{UU}^{\cos(2\phi_h)}|_{\text{Cahn}} = 2 \sum_q e_q^2 x \int d^2 \mathbf{k}_\perp \frac{2(\mathbf{k}_\perp \cdot \hat{\mathbf{h}})^2 - \mathbf{k}_\perp^2}{Q^2} f_q(x, \mathbf{k}_\perp^2) D_q(z, \mathbf{P}_\perp^2), \quad (27)$$

$$F_{UU}^{\cos(2\phi_h)}|_{\text{BM}} = - \sum_q e_q^2 x \int d^2 \mathbf{k}_\perp \frac{P_{hT}(\mathbf{k}_\perp \cdot \hat{\mathbf{h}}) + z[\mathbf{k}_\perp^2 - 2(\mathbf{k}_\perp \cdot \hat{\mathbf{h}})^2]}{2k_\perp P_\perp} \Delta f_{q^\uparrow/p}(x, \mathbf{k}_\perp^2) \Delta D_{h/q^\uparrow}(z, \mathbf{P}_\perp^2). \quad (28)$$

In Eq. (27), light-cone parameters x and z do not exactly coincide with x_{bj} and z_h , and that formula should be considered as an approximation to the full twist-4 contribution to $F_{UU}^{\cos(2\phi_h)}$.

For the TMD parametrizations one often uses a Gaussian ansatz, as also supported by phenomenological analyses in [67], in which $f_q(x, \mathbf{k}_\perp^2)$ and $D_q(z, \mathbf{P}_\perp^2)$ are expressed as

$$f_q(x, \mathbf{k}_\perp^2) = f_q(x) \frac{e^{-k_\perp^2 / \langle k_\perp^2 \rangle}}{\pi \langle k_\perp^2 \rangle}, \quad (29)$$

$$D_q(z, \mathbf{P}_\perp^2) = D_q(z) \frac{e^{-P_\perp^2 / \langle P_\perp^2 \rangle}}{\pi \langle P_\perp^2 \rangle}, \quad (30)$$

where $f_q(x)$ and $D_q(z)$ are the collinear PDFs and FFs respectively.

It is important to emphasize that the Gaussian widths $\langle k_\perp^2 \rangle$ and $\langle P_\perp^2 \rangle$ may have kinematic dependence on x or z , as suggested in the parameterizations shown in Eqs. (16) and (17) and in many other TMD fits. Similarly their flavor dependence, neglected in Ref. [15] as in most phenomenological studies, could play a role [38]. Unfortunately, the scarcity of experimental data on the azimuthal dependence of the unpolarized cross sections, together with the more complicated theoretical framework needed to address it, prevent from reaching an analysis at the same level of sophistication as the one presented in Sec. II B.

In the following we use the LHAPDF CJ15lo set for the collinear PDF [68], and the DSSFFlo set for the collinear FF [69], both employed in [60] for A_{UT} asymmetry studies of the SoLID Preliminary Conceptual Design Report in [28].

The Boer-Mulders TMD function is parametrized as follows:

$$\begin{aligned} \Delta f_{q^\uparrow/p}(x, \mathbf{k}_\perp^2) &= \\ &= \Delta f_{q^\uparrow/p}(x) \sqrt{2e} \frac{k_\perp}{M_{\text{BM}}} e^{-k_\perp^2 / M_{\text{BM}}^2} \frac{e^{-k_\perp^2 / \langle k_\perp^2 \rangle}}{\pi \langle k_\perp^2 \rangle}, \end{aligned} \quad (31)$$

with

$$\begin{aligned} \Delta f_{q^\uparrow/p}(x) &= \\ &= N_q \frac{(\alpha_q + \beta_q)^{(\alpha_q + \beta_q)}}{\alpha_q^{\alpha_q} \beta_q^{\beta_q}} x^{\alpha_q} (1-x)^{\beta_q} f_q(x), \end{aligned} \quad (32)$$

where N_q , α_q , β_q , and M_{BM} are the parameters of the Boer-Mulders quark distributions [70] (see also table 4 in [17]). By imposing $|N_q| \leq 1$, the so-called positivity

bound $-|\Delta f_{q^\uparrow/p}(x, \mathbf{k}_\perp^2)| \leq f_{q/p}(x, \mathbf{k}_\perp^2)$ is satisfied. The Boer-Mulders function can be rewritten also as

$$\begin{aligned} \Delta f_{q^\uparrow/p}(x, \mathbf{k}_\perp^2) &= \\ &= \Delta f_{q^\uparrow/p}(x) \sqrt{2e} \frac{k_\perp}{M_{\text{BM}}} \frac{e^{-k_\perp^2 / \langle k_\perp^2 \rangle_{\text{BM}}}}{\pi \langle k_\perp^2 \rangle}, \end{aligned} \quad (33)$$

with

$$\langle k_\perp^2 \rangle_{\text{BM}} = \frac{\langle k_\perp^2 \rangle M_{\text{BM}}^2}{\langle k_\perp^2 \rangle + M_{\text{BM}}^2}. \quad (34)$$

The Collins FF is parametrized as follows:

$$\begin{aligned} \Delta D_{h/q^\uparrow}(z, \mathbf{P}_\perp^2) &= \\ &= \Delta D_{h/q^\uparrow}(z) \sqrt{2e} \frac{P_\perp}{M_C} e^{-P_\perp^2 / M_C^2} \frac{e^{-P_\perp^2 / \langle P_\perp^2 \rangle}}{\pi \langle P_\perp^2 \rangle}, \end{aligned} \quad (35)$$

with

$$\Delta D_{h/q^\uparrow}(z) = 2N_q^C \frac{(\gamma + \delta)^{\gamma + \delta}}{\gamma^\gamma \delta^\delta} z^\gamma (1-z)^\delta D_q(z), \quad (36)$$

where N_q^C , γ , δ , and M_C are free parameters for the favored and disfavored Collins FFs [71] (see also table 3 in [17]). Even in this case, by imposing $|N_q^C| \leq 1$, the corresponding positivity bound for the Collins function is fulfilled.

By combining the two Gaussians in Eq. (35) we have:

$$\Delta D_{h/q^\uparrow}(z, \mathbf{P}_\perp^2) = \Delta D_{h/q^\uparrow}(z) \sqrt{2e} \frac{P_\perp}{M_C} \frac{e^{-P_\perp^2 / \langle P_\perp^2 \rangle_c}}{\pi \langle P_\perp^2 \rangle_c}, \quad (37)$$

with

$$\langle P_\perp^2 \rangle_c = \frac{\langle P_\perp^2 \rangle M_C^2}{\langle P_\perp^2 \rangle + M_C^2}. \quad (38)$$

These Gaussian parametrizations allow one to carry out all the integrals over the transverse momenta analytically. Thereby, by inserting the above distribution and fragmentation functions into the expressions of the structure functions F_{UU} in Eq. (19), $F_{UU}^{\cos(\phi_h)}|_{\text{Cahn}}$ in Eq. (22), $F_{UU}^{\cos(\phi_h)}|_{\text{BM}}$ in Eq. (23), $F_{UU}^{\cos(2\phi_h)}|_{\text{Cahn}}$ in Eq. (27), and $F_{UU}^{\cos(2\phi_h)}|_{\text{BM}}$ in Eq. (28), we obtain the following set of equations (where we use $x = x_{bj}$ and $z = z_h$, valid within the approximations we consider):

$$F_{UU} = \sum_q e_q^2 x_{bj} f_q(x_{bj}) D_q(z_h) \frac{e^{-P_{hT}^2 / \langle P_{hT}^2 \rangle}}{\pi \langle P_{hT}^2 \rangle}, \quad (39)$$

$$F_{UU}^{\cos(\phi_h)}|_{\text{Cahn}} = -2 \frac{P_{hT}}{Q} \sum_q e_q^2 x_{bj} f_q(x_{bj}) D_q(z_h) \times \frac{z_h \langle k_\perp^2 \rangle}{\langle P_{hT}^2 \rangle} \frac{e^{-P_{hT}^2 / \langle P_{hT}^2 \rangle}}{\pi \langle P_{hT}^2 \rangle}, \quad (40)$$

$$F_{UU}^{\cos(\phi_h)}|_{\text{BM}} = 2e \frac{P_{hT}}{Q} \sum_q e_q^2 x_{bj} \frac{\Delta f_{q^\uparrow/p}(x_{bj})}{M_{\text{BM}}} \frac{\Delta D_{h/q^\uparrow}(z_h)}{M_C} \frac{e^{-P_{hT}^2/\langle P_{hT}^2 \rangle_{\text{BM}}}}{\pi \langle P_{hT}^2 \rangle_{\text{BM}}^4} \frac{\langle k_\perp^2 \rangle_{\text{BM}}^2 \langle P_\perp^2 \rangle_{\text{C}}^2}{\langle k_\perp^2 \rangle_{\text{C}} \langle P_\perp^2 \rangle_{\text{BM}}}$$

$$\times [z_h^2 \langle k_\perp^2 \rangle_{\text{BM}} (P_{hT}^2 - \langle P_{hT}^2 \rangle_{\text{BM}}) + \langle P_\perp^2 \rangle_{\text{C}} \langle P_{hT}^2 \rangle_{\text{BM}}], \quad (41)$$

$$F_{UU}^{\cos(2\phi_h)}|_{\text{Cahn}} = 2 \frac{P_{hT}}{Q^2} \sum_q e_q^2 x_{bj} f_q(x_{bj}) D_q(z_h) \frac{z_h^2 \langle k_\perp^2 \rangle_{\text{BM}}^2}{\langle P_{hT}^2 \rangle_{\text{BM}}^2} \frac{e^{-P_{hT}^2/\langle P_{hT}^2 \rangle}}{\pi \langle P_{hT}^2 \rangle}, \quad (42)$$

$$F_{UU}^{\cos(2\phi_h)}|_{\text{BM}} = -e P_{hT}^2 \sum_q e_q^2 x_{bj} \frac{\Delta f_{q^\uparrow/p}(x_{bj})}{M_{\text{BM}}} \frac{\Delta D_{h/q^\uparrow}(z_h)}{M_C} \frac{e^{-P_{hT}^2/\langle P_{hT}^2 \rangle_{\text{BM}}}}{\pi \langle P_{hT}^2 \rangle_{\text{BM}}^3} \frac{z_h \langle k_\perp^2 \rangle_{\text{BM}}^2 \langle P_\perp^2 \rangle_{\text{C}}^2}{\langle k_\perp^2 \rangle_{\text{C}} \langle P_\perp^2 \rangle_{\text{BM}}}, \quad (43)$$

where

$$\langle P_{hT}^2 \rangle = \langle P_\perp^2 \rangle + z_h^2 \langle k_\perp^2 \rangle,$$

$$\langle P_{hT}^2 \rangle_{\text{BM}} = \langle P_\perp^2 \rangle_{\text{C}} + z_h^2 \langle k_\perp^2 \rangle_{\text{BM}}. \quad (44)$$

Eqs. (39)-(43) and the other related formulas are used for calculating the central values of the unpolarized cross-section pseudo-data with and without the azimuthal modulations in 5D binning of x_{bj} , Q^2 , P_{hT} , z_h and ϕ_h (see Appendix B as well as Appendices A and B in [61]). The pseudo-data are obtained from an event generator package, the original version of which can be found at [60]. In the analysis, we take

$$\langle k_\perp^2 \rangle = 0.604 \text{ (GeV/c)}^2,$$

$$\langle P_\perp^2 \rangle = 0.114 \text{ (GeV/c)}^2, \quad (45)$$

along with all the parameters in Eqs. (39)-(43) taken from [17, 60, 72]: namely,

- $N_u = 0.35$, $N_d = -0.9$, $\alpha_u = 0.73$, $\beta_u = 3.46$,
 $\alpha_d = 1.08$, $\beta_d = 3.46$, $M_{\text{BM}}^2 = 0.34 \text{ GeV}^2$;
- $N_{u, fav}^C = 0.49$, $N_{d, dis}^C = -1.00$, $\gamma = 1.06$, $\delta = 0.07$,
 $M_C^2 = 1.50 \text{ GeV}^2$.

Notice that the choice in Eq. (45) is somewhat consistent with the findings in MPTMD24 (see the mean values of flavor-independent pink points in Fig. 19 of Ref. [38]) and similar to Set V of parameters discussed in Ref. [73].

We also note that while in the structure function F_{UU} , the Gaussian widths for the unpolarized TMD PDFs and TMD FFs enter only in a specific combination (see Eq. (44)), in both Cahn contributions, Eqs. (40) and (42), $\langle k_\perp^2 \rangle$ appears explicitly. This means that more precise data in specific/extended kinematical regions will offer an important and complementary tool for the study of these properties.

III. NUCLEAR EFFECTS FROM FERMI MOTION

We consider here possible sources of nuclear effects to estimate their effect on the process under investigation.

Indeed, in the ^3He rest frame the initial-state nucleon entering the SIDIS process in Eq. (1) is not at rest due to its Fermi motion. This intrinsic motion modifies the kinematics relative to the scattering off a stationary neutron (or proton) in the laboratory frame, shifting, in particular, the variables x_{bj} , P_{hT} , and z_h . Consequently, this can affect the extraction of the transverse momentum widths $\langle k_\perp^2 \rangle$ and $\langle P_\perp^2 \rangle$ (see e.g., Eq. 45). Within the kinematic ranges considered here and relevant to the proposal in Ref. [61], we have found that the differences in x_{bj} , P_{hT} , and z_h due to the Fermi motion can lead to average changes of approximately 20%, as illustrated by ratio plots in Figs. 3–5¹.

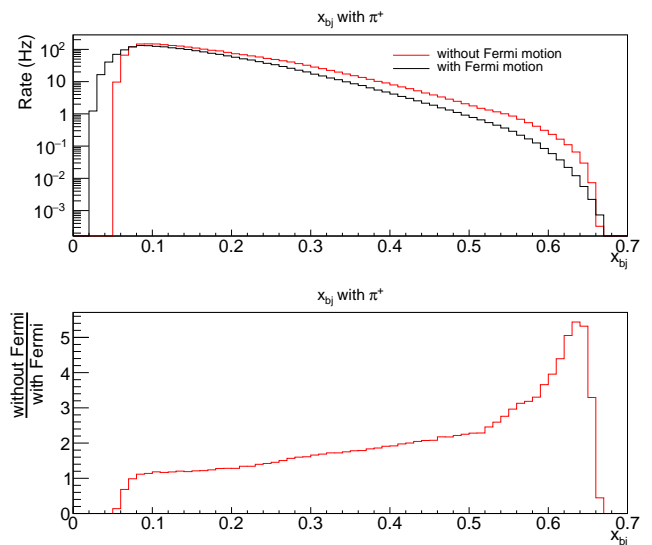


FIG. 3. Upper panel: x_{bj} distributions of generated events' rate for π^+ as leading hadron, with (black histogram) and without (red histogram) Fermi motion of the initial nucleon in the ^3He target. Lower panel: their ratio.

¹ These results refer to the production of positively charged pions at 11 GeV electron beam energy.

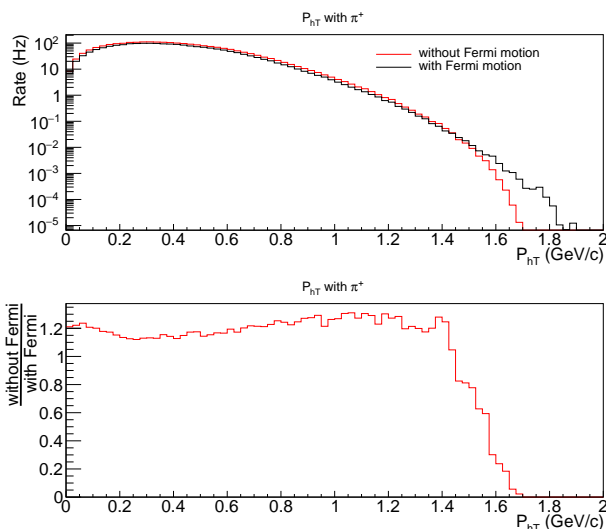


FIG. 4. The first plot displays the P_{hT} distributions of generated events' rate for π^+ as leading hadron, with (black histogram) and without (red histogram) Fermi motion of the initial nucleon in the ${}^3\text{He}$ target, whereas the second plot shows their ratio.

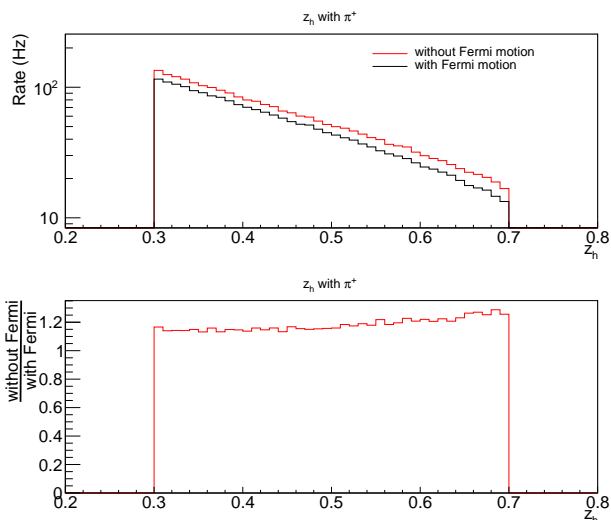


FIG. 5. The first plot displays the z_h distributions of generated events' rate for π^+ as leading hadron, with (black histogram) and without (red histogram) Fermi motion of the initial nucleon in the ${}^3\text{He}$ target, whereas the second plot shows their ratio.

In particular, modifications in P_{hT} directly impact the extracted transverse momentum widths, according to Eq. (20). In this case, the obtained correlation between P_{hT} values with and without Fermi motion is shown in Fig. 6 (see also Fig. 7). Furthermore, the comparison of the P_{hT} distributions with and without Fermi motion – using π^\pm as the leading hadron – shows that the smearing effect on P_{hT} is approximately ± 0.014 GeV/c. As shown in [61], one can see that the results of Figs. 3, 4, 6, and 7 are quite similar to those of π^- as lead-

ing hadron. This smearing translates to uncertainties of ± 0.0006 (GeV/c) 2 in the extracted $\langle k_\perp^2 \rangle$, as well as ± 0.0001 (GeV/c) 2 in $\langle P_\perp^2 \rangle$. These results indicate that while the Fermi motion introduces non-negligible effects, those can be properly quantified and systematically studied. In the proposed data analyses of the future SoLID SIDIS experiments E12-10-006 and E12-11-007, appropriate correction procedures to account for the Fermi motion effects will be implemented, ensuring accurate extraction of the intrinsic transverse momentum distributions. Nevertheless, the impact of the nuclear effects based on the Fermi motion (within the current ansatz) on the statistical uncertainty part of the SoLID pseudo-data has been studied and found to be negligible as compared to the total uncertainties or, even the systematic uncertainties (see Appendix A), and therefore does not affect the physics impact results shown in Sec. IV.

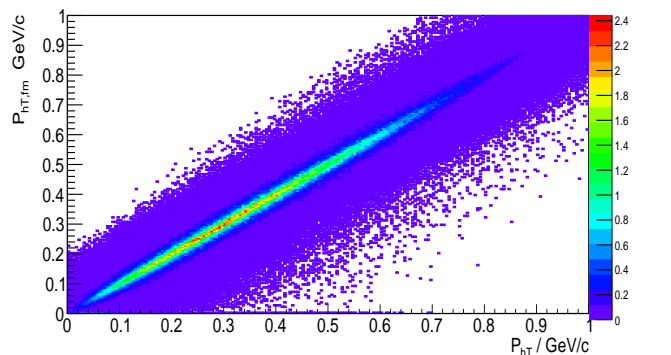


FIG. 6. A 2D plot showing the P_{hT} distribution with Fermi motion versus without Fermi motion of the initial nucleon in the ${}^3\text{He}$ target for π^+ as the leading hadron, weighted by the cross section \times acceptance.

We also note that in the study of neutron single spin asymmetries from SIDIS off a transversely polarized ${}^3\text{He}$ target at the SoLID SIDIS kinematics [74], it was shown that the Fermi motion and binding effects can be properly taken into account via a simple procedure: more precisely, the only nuclear structure ingredients turn out to be the nucleon effective polarizations (quantities known from precise few-body calculations in a rather model independent way).

Furthermore, more recently, Liu and collaborators [72], focusing on unpolarized SIDIS off light nuclei, have shown that the conventional nuclear effect on the unpolarized structure function can be at a few percent level and even smaller for the azimuthal asymmetry. These results may provide a baseline for new studies of other exotic nuclear effects and serve as an estimate for nuclear corrections in experimental analyses of future data involving light nuclear targets (such as the proposed SoLID SIDIS data analyses of [32], [34], and [61]).

The approved run-group proposal [61] and this paper may motivate more theoretical studies of nuclear effects in SIDIS processes with a ${}^3\text{He}$ target. Together with

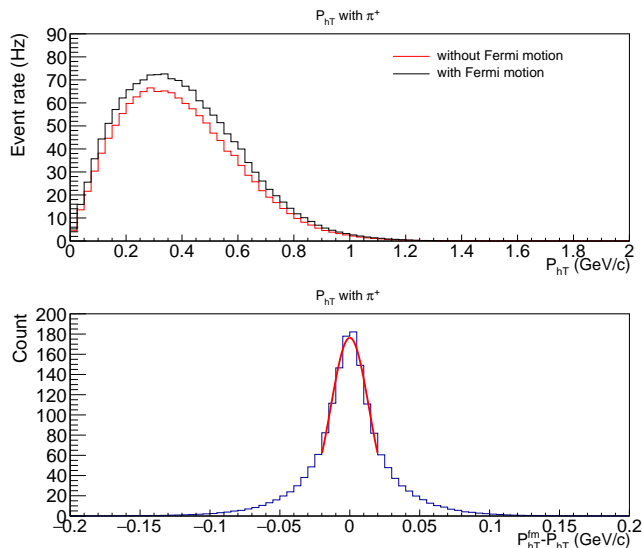


FIG. 7. Upper panel: P_{hT} distribution with and without Fermi motion of the initial nucleon in the ${}^3\text{He}$ target for π^+ as leading hadron. Lower panel: their difference.

the data, these new studies will not only enable reliable extractions of the information on the neutron, but also further investigation of possible EMC effect [75–77] in TMD physics.

IV. PHYSICS IMPACT STUDIES

In this section we present our projections and MAPTMD24+SoLID physics impact results on the unpolarized cross section, including the SoLID statistical and systematic uncertainties (see Appendix A and Ref. [61]).

Adopting the MAPTMD24 framework [38], as elaborated in Sec. II B, we show the impact of the SoLID pseudo-data on the unpolarized TMDs (extracted in the analysis of the MAP Collaboration) in Sec. IV C in particular.

A. SoLID SIDIS kinematics

In our study we have used the following kinematic-variable ranges of the pseudo-data sets given as

$$0 < x_{bj} < 0.7, \quad 0.3 < z_h < 0.7, \quad Q^2 > 1.4 \text{ GeV}^2,$$

$$P_{hT} < \min[\min[0.2Q, 0.5z_hQ] + 0.3 \text{ GeV}, z_hQ].$$

In Fig. 8 we show the correlations between different kinematic variables (equivalently, the phase-space components) obtained taking into account the SoLID acceptance but without imposing the z_h cut. More precisely, we present the correlations in the phase space at the combined 11 GeV and 8.8 GeV beam energies for π^+ production off transversely polarized ${}^3\text{He}$ target.

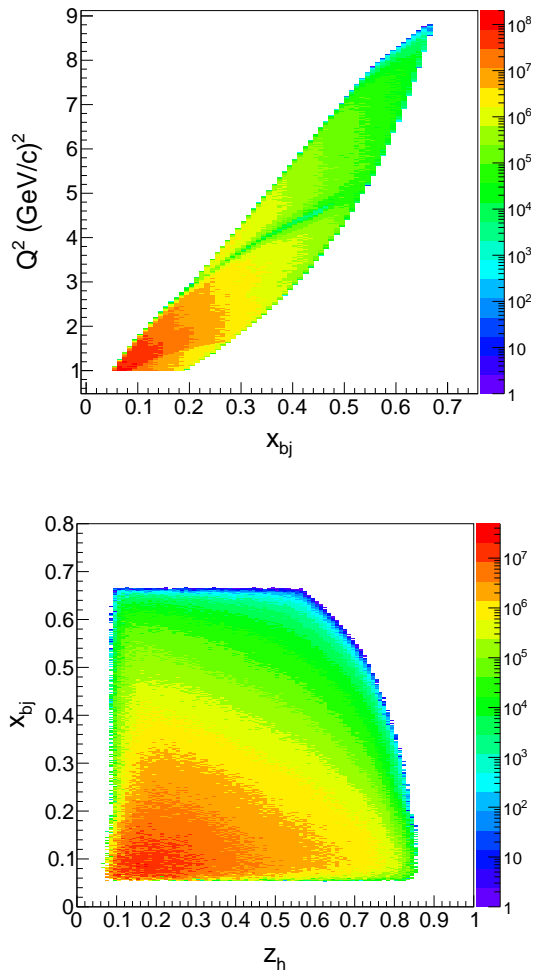


FIG. 8. Phase-space correlations for the SoLID apparatus between Q^2 and x_{bj} (top plot), x_{bj} and z_h (bottom plot). The SoLID z_h cut is not applied.

B. Transverse momentum projections for the SIDIS unpolarized cross section

We start by considering the SoLID projections of the SIDIS unpolarized cross section (see Eq. (3)) integrated over ϕ_h as a function of P_{hT} for π^+ . Examples of such projections are shown in Figs. 9 and 10. The pseudo-data points in both figures include the SoLID statistical and systematic uncertainties combined in quadrature, and the central values are determined by employing the MAPTMD24 framework (more details are collected in Sec. IV C). In all the panels of both figures, the pseudo-data are simulated at 11 GeV. In addition, in Appendix B, where the central values of the projections are obtained using the general ansatz of a simpler TMD parton model discussed in Sec II C, we show results both at 11 GeV and 8.8 GeV.

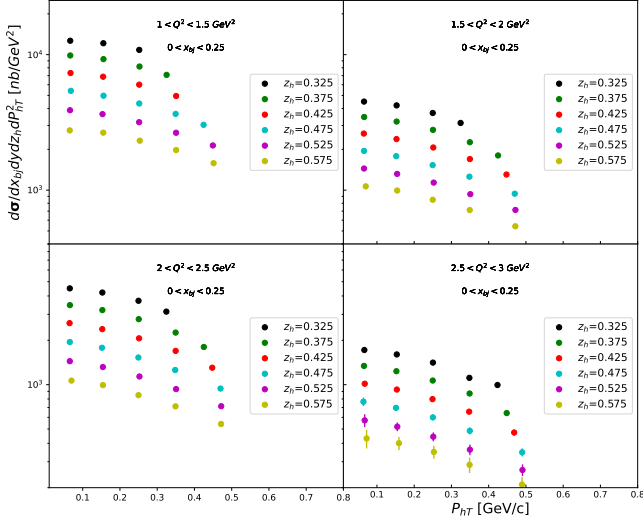


FIG. 9. Unpolarized cross section for π^+ production at beam energy 11 GeV as a function of P_{hT} , in specific x_{bj} and Q^2 kinematic bins, and at given z_h values within the range of $[0.3, 0.7]$.

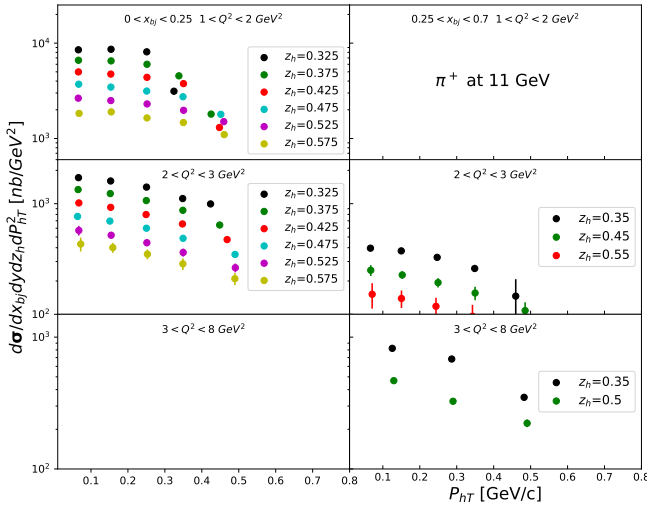


FIG. 10. Unpolarized cross section for π^+ production at beam energy 11 GeV as a function of P_{hT} , as in Fig. 9 but for larger two x_{bj} and three Q^2 kinematic bins, and at given z_h values within the range of $[0.3, 0.7]$.

C. Impact results on unpolarized TMDs and FFs

The unpolarized TMD-related impact results are shown in Fig. 11 (for π^\pm and K^\pm), as well as in Appendix C, in Fig. C1 (for π^\pm) and in Fig. C2 (for K^\pm). All figures are obtained at $Q^2 = 2 \text{ GeV}^2$. Qualitatively similar results are also obtained at other values of Q^2 available at SoLID: namely, for 4 and 6 GeV^2 [61]. Each column refers to a fixed x_{bj} value: namely, 0.05, 0.1, 0.3 and 0.5, while each row refers to a given quark flavor in the MAPTMD24 ansatz, where the flavors considered are u ,

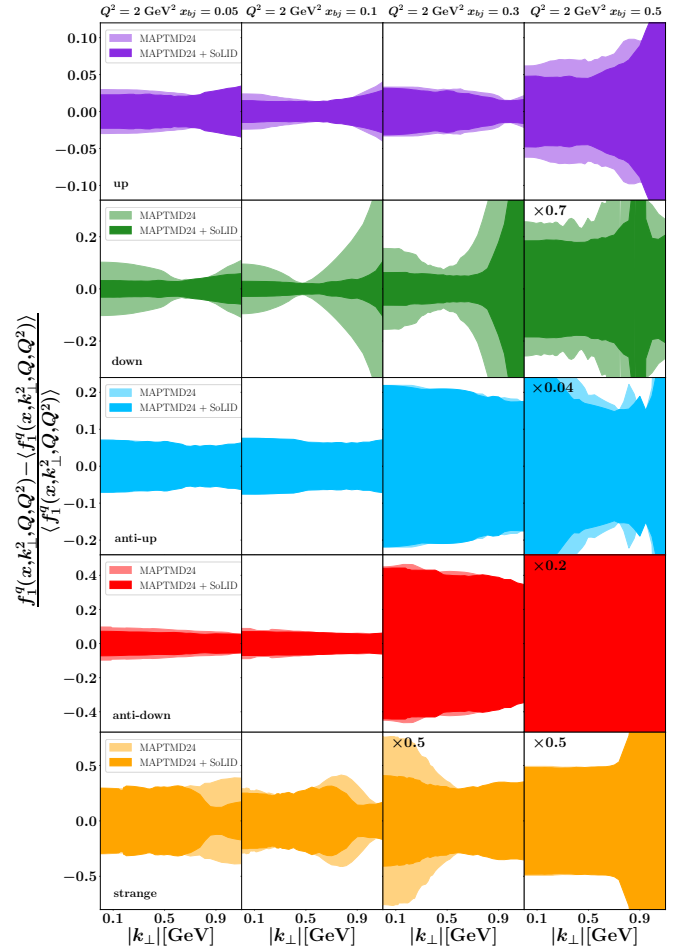


FIG. 11. The MAPTMD24 and impact MAPTMD24+SoLID results on unpolarized TMDs for the final-state pions & kaons configuration in the bins of $x_{bj} = 0.05$, $x_{bj} = 0.1$, $x_{bj} = 0.3$, $x_{bj} = 0.5$ at $Q^2 = 2 \text{ GeV}^2$ as a function of $|k_\perp|$. See the text in this section for more details.

d , \bar{u} , \bar{d} , and s . In the vertical axis we have the relative difference of the unpolarized TMD f_1^q with respect to the average value ($\langle f_1^q \rangle$) of the ensemble of replicas from the MAPTMD24 (light bands) and the MAPTMD24+SoLID (dark bands) analyses, so defined:

$$\frac{f_1^q(x_{bj}, k_\perp^2, Q, Q^2) - \langle f_1^q(x_{bj}, k_\perp^2, Q, Q^2) \rangle}{\langle f_1^q(x_{bj}, k_\perp^2, Q, Q^2) \rangle}. \quad (46)$$

The horizontal axis shows the modulus of the quark intrinsic transverse momentum $|k_\perp|$. The light and dark uncertainty bands are computed at 68% confidence level (CL).

One can see that the main impact, coming from the SoLID ^3He pseudo-data, is on the d -quark distribution. This is because the experimental data used in the MAPTMD24 analysis are for proton and deuteron targets and do not provide constraints in the SoLID kinematic region. In contrast, the u -quark TMD is already well constrained by the available data, except in the large-

x region ($x_{bj} \simeq 0.5$). It is important to stress that the uncertainties obtained in our study, by using the SoLID pseudo-data of the π^\pm & K^\pm configuration, could be similar or, slightly larger than the uncertainties obtained by using only the pseudo-data of π^\pm . This can be traced back to the following issues: (i) unavoidable intrinsic uncertainty stemming from the used collinear PDF sets; (ii) correlations coming from having similar TMDs but different cross sections in certain regions; (iii) specific number of replicas that is fixed by the MAPTMD24 extraction.

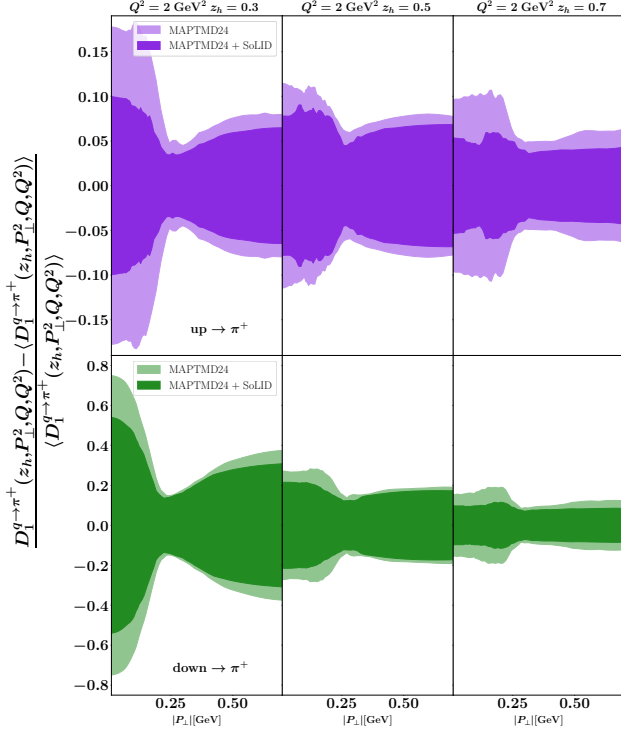


FIG. 12. The MAPTMD24 and impact MAPTMD24+SoLID results on unpolarized FFs for the final-state pions in the bins of $z_h = 0.3, z_h = 0.5, z_h = 0.7$ at $Q^2 = 2 \text{ GeV}^2$ as a function of $|P_\perp|$. See the text in this section for more details.

For completeness, in Figs. 12 and 13 we show the impact study on the pion and kaon TMD FFs, the complementary nonperturbative key element in SIDIS. The quantity under consideration is the corresponding one appearing in Eq. (46), which is

$$\frac{D_1^{q \rightarrow h}(z_h, P_\perp^2, Q, Q^2) - \langle D_1^{q \rightarrow h}(z_h, P_\perp^2, Q, Q^2) \rangle}{\langle D_1^{q \rightarrow h}(z_h, P_\perp^2, Q, Q^2) \rangle}. \quad (47)$$

More in detail, in Fig. 12 we present the results for the favored ($u \rightarrow \pi^+$) and disfavored ($d \rightarrow \pi^+$) pion TMD FFs² at fixed scale, $Q^2 = 2 \text{ GeV}^2$, for different values of

² Here favored (disfavored) refers to the case where the hadron contains (does not contain) the fragmenting quark as a valence quark.

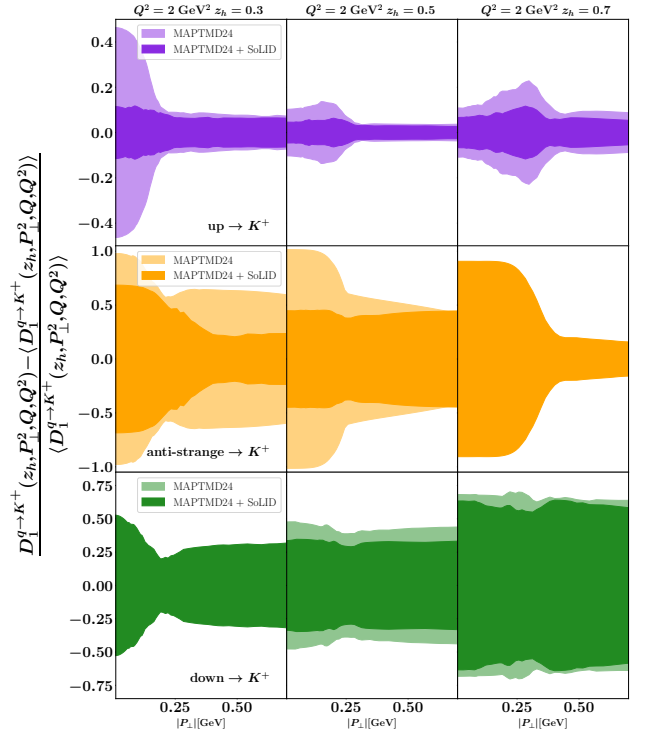


FIG. 13. The MAPTMD24 and impact MAPTMD24+SoLID results on unpolarized FFs for the final-state kaons in the bins of $z_h = 0.3, z_h = 0.5, z_h = 0.7$ at $Q^2 = 2 \text{ GeV}^2$ as a function of $|P_\perp|$. See the text in this section for more details.

z_h as a function of $|P_\perp|$. Similarly, in Fig. 13 we show the results for the three relevant kaon TMD FFs, namely $u \rightarrow K^+$, $\bar{s} \rightarrow K^+$ (both favored) and $d \rightarrow K^+$ (disfavored) for the same Q^2 and z_h values. As one can see even in the case of TMD FFs the reduction in the uncertainties is significant, showing once again the impact of the SoLID analysis.

D. TMD width parameters

1. Results from the parton model analysis of azimuthal modulations

In this section we consider the SoLID pseudo-data for the ϕ_h distributions and try to fit them with a simple function, $A(1 - B \cdot \cos(\phi_h) - C \cdot \cos(2\phi_h))$, to evaluate the azimuthal modulation effects. In this formula, the parameters B and C indicate the amplitudes of the modulation and are directly related to the structure functions entering Eq. (3), while the parameter A is related to F_{UU} . By applying the corresponding simplified fitting, e.g., to the ϕ_h -dependent π^+ pseudo-data from Fig. B1 (and π^- pseudo-data from Fig. A9 in Appendix A of [61]) we obtain the results shown in Figs. 14 and 15.

These azimuthal modulation effects can be analyzed within a simplified TMD approach (Eqs. (19), (21)-(23),

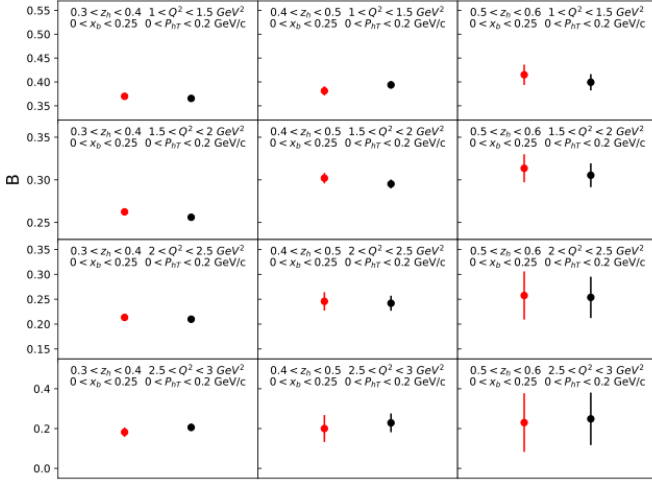


FIG. 14. The parameter B at fixed x_{bj} and P_{hT} bins for different z and Q^2 bins (see the legend) as obtained by using the fitting functional form of $A(1 - B \cdot \cos(\phi_h) - C \cdot \cos(2\phi_h))$. The red and black circle points represent the results for π^+ and π^- production channels, respectively.

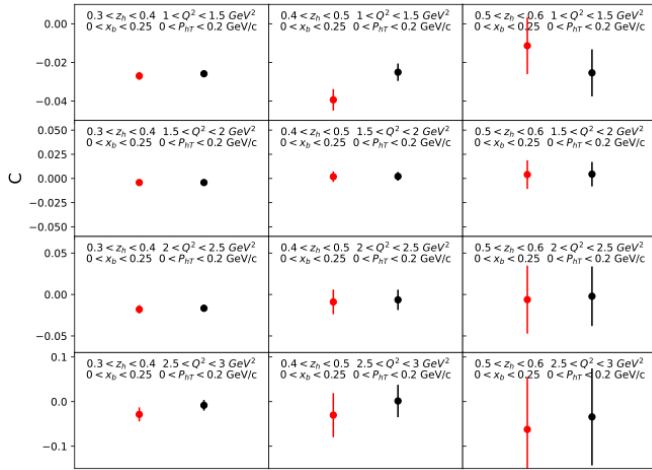


FIG. 15. The parameter C at fixed x_{bj} and P_{hT} bins for different z and Q^2 bins (see the legend) as obtained by using the fitting functional form of $A(1 - B \cdot \cos(\phi_h) - C \cdot \cos(2\phi_h))$. The red and black circle points represent the results for π^+ and π^- production channels, respectively.

(26)-(28)); then, by adopting the Gaussian ansatz of Sec. II C, the intrinsic transverse momentum widths can be extracted from the relative magnitudes of the structure functions F_{UU} , $F_{UU}^{\cos(\phi_h)}$ and $F_{UU}^{\cos(2\phi_h)}$ (Eqs. (39)-(44)). Notice that the two structure functions controlling the azimuthal modulations involve two contributions: the Cahn effect, Eqs. (22) and (27), and the less dominant Boer-Mulders effect, Eqs. (23) and (28).

As one can see from Fig. 14, the parameter B is sizable (around 20-30%) and, at least, for the lower and intermediate z bins (left and central panels), with very small errors. Taking into account the explicit role of the $\langle k_{\perp}^2 \rangle$

width in the Cahn effect (Eq. (40)) entering this term, this quantity could be extremely useful and effective in the extraction of the Gaussian widths.

By substituting the expressions of the final (convoluted) structure functions from Eqs. (39)-(44) into the SIDIS cross section in Eq. (3), we obtain a fitting function in terms of the two intrinsic width parameters, $\langle k_{\perp}^2 \rangle$ and $\langle P_{\perp}^2 \rangle$. In order to carry out the projections with this fitting function we also use the (initial) values from Eq. (45). The fitting is performed for pion production with all the available SoLID pseudo-data (employed to make all the figures in Appendices A and B of [61]), including the systematic uncertainties and using the Least Squares method. The final results, presented by three contours with confidence levels of 68%, 90% and 99% are shown in Fig. 16. The central values and their corresponding uncertainties for the 68% CL are determined as

$$\begin{aligned} \langle k_{\perp}^2 \rangle &= 0.5868 \pm 0.0015 \text{ (GeV/c)}^2, \\ \langle P_{\perp}^2 \rangle &= 0.1166 \pm 0.0002 \text{ (GeV/c)}^2. \end{aligned} \quad (48)$$

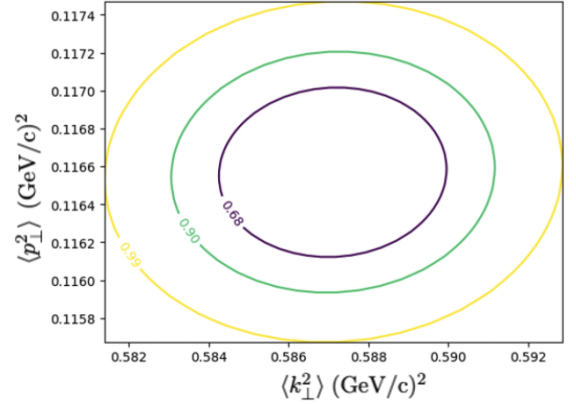


FIG. 16. Three fitting contours for the Gaussian intrinsic width parameters, $\langle k_{\perp}^2 \rangle$ and $\langle P_{\perp}^2 \rangle$, obtained for pion production using the functional form of the total SIDIS unpolarized cross section in Eq. (3). Both Cahn and Boer-Mulders contributions are included.

It is relevant to note that irrespective of the initial values used for the width parameters (which could be different from those adopted here), the obtained approximate result shows how one can significantly improve the accuracy in extracting this information. Thus, by measuring the unpolarized cross section with and without the azimuthal modulations, we will be able to extract the Gaussian width parameters $\langle k_{\perp}^2 \rangle$ and $\langle P_{\perp}^2 \rangle$. The extraction can therefore be carried out by fitting these two parameters to future data (using the functional forms given by Eqs. (39)-(44) or, by new updated formulas within an improved TMD framework).

2. Results from the NLO MAP analysis of the unpolarized cross sections

We now move to a more sophisticated analysis focusing on the unpolarized cross sections within a proper TMD framework. We will then estimate the impact of the SoLID on the extraction of the widths of the distributions using the prescription from Ref. [78] of MAP collaboration:

$$\langle \mathbf{k}_\perp^2 \rangle_r^q(x_{bj}, Q) = \frac{2M_N^2 \hat{f}_1^{q(1)}(x_{bj}, \mathbf{b}_T^2, Q, Q^2)}{\hat{f}_1^q(x_{bj}, \mathbf{b}_T^2, Q, Q^2)} \Big|_{|\mathbf{b}_T|=2b_{\max}}, \quad (49)$$

where the subscript r in the l.h.s. refers to the *regularized* definition of the average squared momenta, where \hat{f}_1^q is the Fourier transform of the TMD PDF, and $\hat{f}_1^{q(1)}$ is its first Fourier moment [79]. Analogously, one could apply similar arguments to the *regularized* average squared transverse momentum for a final hadron h in the fragmentation of a quark q [55, 78–80]:

$$\langle \mathbf{P}_\perp^2 \rangle_r^{q \rightarrow h}(z_h, Q) = \frac{2z_h^2 M_h^2 \hat{D}_1^{q \rightarrow h(1)}(z_h, \mathbf{b}_T^2, Q, Q^2)}{\hat{D}_1^{q \rightarrow h}(z_h, \mathbf{b}_T^2, Q, Q^2)} \Big|_{|\mathbf{b}_T|=2b_{\max}}, \quad (50)$$

where $\hat{D}_1^{q \rightarrow h}$ is the Fourier transform of the TMD FF defined in Eq. (9), and $\hat{D}_1^{q \rightarrow h(1)}$ is the first Bessel moment [79] of the TMD FF.

In Fig. 17 we present the contour bands at 68% CL of the average squared transverse momenta for the unpolarized TMD PDF and the TMD FF for a π^+ at fixed $Q^2 = 2 \text{ GeV}^2$ and $z_h = 0.5$, for different x_{bj} values: $x_{bj} = 0.1, 0.3$ and 0.5 . Namely, we show $\langle \mathbf{P}_\perp^2 \rangle_r^{q \rightarrow \pi^+}$ versus $\langle \mathbf{k}_\perp^2 \rangle_r^q$ for the u and d quark flavors. The results are displayed for different ensembles of replicas with and without SoLID.

As one can see the uncertainties are strongly reduced, in all regions. Notice that these results cannot be directly compared with those shown in the previous subsection, since here we have both the x_{bj}/z_h as well as the flavor dependence. Another method of studies of average values of $\langle \mathbf{k}_\perp^2 \rangle_r^q$ and $\langle \mathbf{P}_\perp^2 \rangle_r^q$ was proposed in Ref. [81] and can be employed on the real data of for estimations of the impact.

Ultimately, the future experimental data will be important to disentangle those dependencies.

V. CONCLUSION AND DISCUSSION

In this paper we have presented the impact study results for the unpolarized SIDIS cross-section off ^3He target based on the approved proposal of Ref. [61], where further details can be found. In particular, the general results include π^+ and π^- pseudo-data with the SoLID statistical uncertainties and theoretical central points projected into selected bins of $(x_{bj}, P_{hT}, z_h, Q^2, \phi_h)$ within

SoLID kinematics, along with the systematic uncertainties evaluated for the acceptance correction, detection and identification of charged particles, radiative corrections, luminosity determination, and other sources. Charged-kaon contributions are considered as well. The SoLID systematic uncertainties are determined and assigned to the unpolarized (azimuthal-integrated) cross-section pseudo-data, without taking into account the azimuthal modulations. On the other hand, the results for the cross section including the azimuthal modulation terms are computed taking into account only the SoLID statistical uncertainties.

For the azimuthal-integrated cross section we adopt the advanced MAPTMD24 framework with TMD evolution up to $N^3\text{LL}$ accuracy (see Sec. II B), whereas for the azimuthal angular-dependent cross section we employ a simpler TMD model (Generalized Parton Model), in which the transverse momentum dependence of TMDs is factorized and modeled in terms of Gaussians (see Sec. II C). Though the latter approach is perhaps too simple to describe the experimental data, it can still be helpful to assess the experimental precision.

Summarizing, in the paper we have presented physics impact results from the combined MAPTMD24+SoLID ansatz on the unpolarized TMDs as a function of $|\mathbf{k}_\perp|$ (for the PDFs) and $|\mathbf{P}_\perp|$ (for the FFs, both for pions and kaons) extracted in the MAPTMD24 framework (see Sec. IV C and Appendix C). Besides, we show results on the (Gaussian) width parameter extraction using the MAPTMD24+SoLID joint fit (see Sec. IV D 2), as well as their approximate results within a simplified TMD ansatz. We also present projection results of the SoLID pseudo-data on the unpolarized cross section as a function of P_{hT} in various bins, showing the SoLID statistical and systematic uncertainties and central values as obtained employing the MAPTMD24 framework (see Sec. IV B). The total systematic uncertainties (Table I and Table II, Appendix A) are applied only to the azimuthal-integrated cross sections, whereas the statistical uncertainties are applied to both cases³. In addition, Appendix B shows several projection results on the unpolarized cross section as a function of ϕ_h in various bins showing the SoLID statistical and systematic uncertainties, as well as central values obtained in the simplified TMD ansatz.

We have also discussed some results from the study on the effect of Fermi motion on the nucleon inside ^3He . It has been found that the impact of this effect on the statistical uncertainty part of the SoLID pseudo-data is negligible as compared to the total uncertainties. However, more studies related to nuclear effects is currently ongoing. It is also important to mention that our proposed experiment will play an important role for the

³ In the future, when a more accurate model becomes available, we will address the total systematic uncertainty of the unpolarized azimuthal angular-dependent cross section (expected to be of the same order of magnitude as that of the azimuthal-integrated cross section).

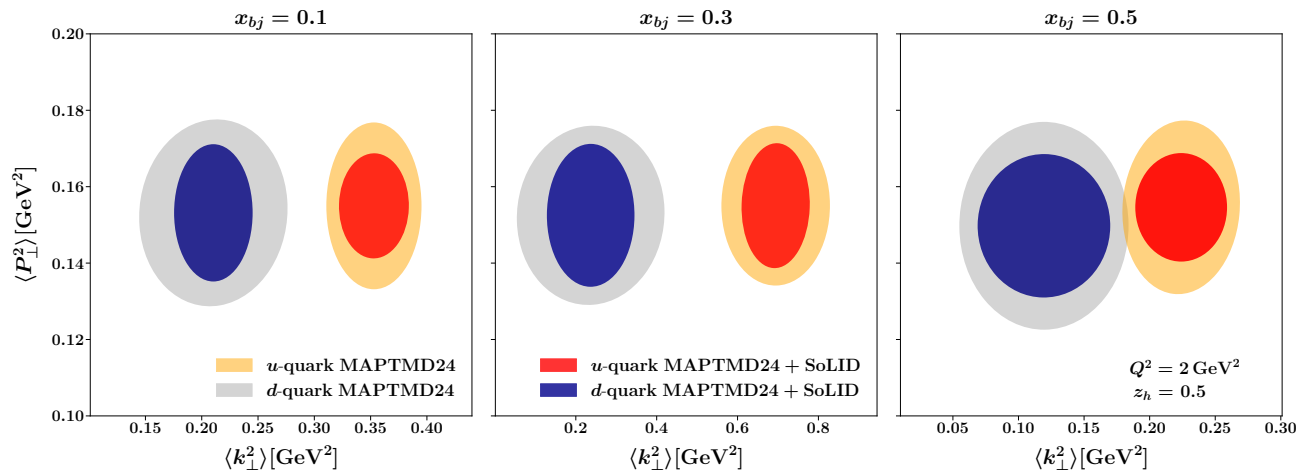


FIG. 17. The contour bands at 68% CL of $\langle P_{\perp}^2 \rangle_r^{q \rightarrow \pi^+}$ as a function of $\langle k_{\perp}^2 \rangle_r^q$, obtained from the fit of MAPTMD24 and joint fit of MAPTMD24+SoLID for the u (purple curves) and d (green curves) quark flavors at fixed $z_h = 0.5$ and $Q^2 = 2 \text{ GeV}^2$. The three panels correspond to three values of x_{bj} : $x_{bj} = 0.1$ (left panel), $x_{bj} = 0.3$ (central panel) and $x_{bj} = 0.5$ (right panel).

global studies of the EMC effect [75–77], which addresses the differences in the partonic structure of a free proton and a bound proton in a nucleus. There are several possible explanations for the EMC effect, including the non-negligible Fermi motion of the nucleon, short-range correlations, the off-shellness of the bound nucleon and nuclear medium modifications. Combined with data on proton cross section [38, 78, 82–84], the neutron cross section can be extracted using the state-of-the-art calculation [85] for treating the ^3He nuclear effect. Both in our projections and MAPTMD24+SoLID physics impact results, we have used the impulse approximation, in which the ^3He is treated as a system of two protons plus one neutron. The extracted neutron results can then be compared to available and future data on deuterium target as well as upcoming results from various global analyses, which will allow for an improved investigation of the EMC effect in SIDIS processes considering the scattering off a ^3He target.

ACKNOWLEDGMENTS

The work of H.G., S.J., V.K., Z.Z. is supported by the U.S. Department of Energy contract No. DE-FG02-03ER41231. The work of M.C., A.P., J.-P.C. is supported by the U.S. Department of Energy contract No. DE-AC05-06OR23177, under which Jefferson Science Associates, LLC operates Jefferson Lab, and the National Science Foundation under Grants No. PHY-2310031, No. PHY-2335114 (A.P.). The work of Y.T. is supported by the U.S. Department of Energy contract No. DE-FG02-84ER40146. The work of U.D. is supported by the European Union “Next Generation EU” program through the Italian PRIN 2022 grant n. 20225ZHA7W. The work of L.R. is partially supported by the Italian Ministero dell’Università e Ricerca (MUR) through the

research grant 20229KEFAM (PRIN2022, Next Generation EU, CUP H53D23000980006).

Appendix A: Systematic uncertainties of the unpolarized cross section with F_{UU}

In this appendix we present a summary of all SoLID systematic uncertainty sources studied and discussed in Sec. 5 of the experimental proposal of Ref. [61]; the magnitudes of the assigned systematic uncertainties are listed in Table I (for pions) and Table II (for kaons).

The total systematic uncertainty of the unpolarized cross section for charged pion production is up to 11%, calculated by rounding off the quadrature sum of the individual contributions. The largest source of uncertainty comes from the so-called coincidence acceptance correction being 8.2% (which includes the electron acceptance correction uncertainty). One should also note that the π^+ and π^- systematic uncertainties are determined to be approximately similar by their magnitudes. It is the case for both π^+ and π^- at low- Q^2 and high- Q^2 regions as well. It is the reason why we consider only one total systematic uncertainty for both particles and for the entire Q^2 region, from low Q^2 to high Q^2 .

It is essential to emphasize that for the unpolarized cross section for charged kaons all the systematic uncertainty sources, except for the coincidence acceptance correction and the charged-hadron detection efficiency, is the same as shown in Table I for charged pion production. Meanwhile, for the kaons, the systematic uncertainty of the

- (i) coincidence acceptance correction is evaluated in a similar way as the acceptance correction for the pions discussed in Sec. 5.1.3 of [61].

Sources	Uncertainty
Coincidence acceptance correction	8.2%
Experimental resolution	3.5%
Pion detection efficiency	4%
Electron detection efficiency	< 2%
Radiative corrections	2.1%
Vector meson production	1%
Luminosity determination	$\lesssim 3\%$
Total	$\lesssim 11\%$

TABLE I. Systematic uncertainty budget of the unpolarized cross section for the produced (final-state) charged pions.

- (ii) detection efficiency is evaluated in a similar way as the efficiency for the pions discussed in Sec. 5.3.1 of [61].

Thereby, the total systematic uncertainty of the unpolarized cross section for produced charged kaons is determined to be up to 18%, calculated by the quadrature sum of the individual contributions as shown in Table II.

Sources	Uncertainty
Coincidence acceptance correction	$\sim 13\%$
Experimental resolution	3.5%
Kaon detection efficiency	11%
Electron detection efficiency	< 2%
Radiative corrections	2.1%
Vector meson production	1%
Luminosity determination	$\lesssim 3\%$
Total	$\lesssim 18\%$

TABLE II. Systematic uncertainty budget of the unpolarized cross section for the produced (final-state) charged kaons.

In our proposed experiment, there will also be one hour of data collection on a H₂ target at both 2.2 GeV and 4.4 GeV beam energies for the purpose of collecting elastic scattering data during the future SoLID data acquisition period. This will allow us to reassess the acceptance correction aspect of the current systematic uncertainty analysis, by having the SoLID elastic data at our disposal. With high-precision elastic data (from H₂ reference cell runs) and with possibly improved theoretical models, approximately five-ten years from now, we may even have systematic uncertainty re-estimation for the acceptance correction to be much smaller than what is shown in Table I and Table II. Our perspective on a better re-evaluation of this component of the total systematic uncertainty is also based on actual detector characteristics: large acceptance, high luminosity and kinematic range of the SoLID apparatus, by which it will have better performance in cross-section measurements as compared to BigBite and CLAS12 detectors at JLab. In the case of kaons, the large systematic uncertainty of the 13% coincidence acceptance correction arises primarily from the limited analysis currently available. To improve this estimate, we plan to incorporate results from

the upcoming CLAS12 charged kaon SIDIS analysis [86], which is expected to be published prior to the start of SoLID data taking.

Eventually, due to the total systematic uncertainty reduction for both pions and kaons, we will have improved SoLID SIDIS impact results from the MAP ansatz compared to what is shown in Fig. 11 and Figs. C1, C2. Besides, the scatter plots of average squared transverse momenta in Fig. 17 will be remade as well, with more precise determinations of $\langle P_{\perp}^2 \rangle_r$ and $\langle k_{\perp}^2 \rangle_r$.

Appendix B: Azimuthal-angle projections of the SoLID SIDIS unpolarized cross section at low- Q^2 region from the general ansatz of Sec. II C

By utilizing the simplified TMD framework from Sec. II C, we can have some insight into azimuthal modulation effects, by adopting the given Gaussian ansatz, where intrinsic transverse momentum widths in the unpolarized SIDIS process come from the relative magnitudes of the structure functions F_{UU} , $F_{UU}^{\cos(\phi_h)}$, and $F_{UU}^{\cos(2\phi_h)}$.

In this regard, we consider three scenarios that have been used in a data comparison in the analysis of Ref. [49, 50], where two of them give good agreement with data in many bins. Namely,

- the model considered in Barone2015 [15, 49] with $\langle k_{\perp}^2 \rangle = 0.037$ (GeV/c)² and $\langle P_{\perp}^2 \rangle = 0.126 + 0.506z_h^2$ (GeV/c)². Within this model, the outgoing hadron's transverse momentum is mainly due to the fragmentation process. The P_{\perp}^2 parametrization gives a good description of the unpolarized SIDIS cross-section data from [49] and HERMES data on multiplicities [15].
- the model considered in Bacchetta2011 [53] with $\langle k_{\perp}^2 \rangle = 0.14$ (GeV/c)² and $\langle P_{\perp}^2 \rangle = 0.42 z_h^{0.54} (1 - z_h)^{0.37}$ (GeV/c)². This model too allows for a good description of the unpolarized SIDIS cross-section and HERMES multiplicity data.

In order to generate the unpolarized cross-section pseudo-data in the simplified TMD framework, we adopt another approach that is very close to Barone2015 model but without any z_h dependence in $\langle P_{\perp}^2 \rangle$. We call it the Default model taking $\langle k_{\perp}^2 \rangle = 0.604$ (GeV/c)² and $\langle P_{\perp}^2 \rangle = 0.114$ (GeV/c)² (see Eq. (45)). The Default, Barone2015 and Bacchetta2011 models are expected to render similar physics representations.

We show here some of our results at low Q^2 , see Figs. B1, B2, B3, B4 (see also Appendices A and B of Ref. [61] for more figures)⁴. In all these multi-binned fig-

⁴ For the unpolarized cross-section expression (with the Default model) see Eq. (3), along with Eqs. (39)-(44), Eq. (21) and Eq. (26).

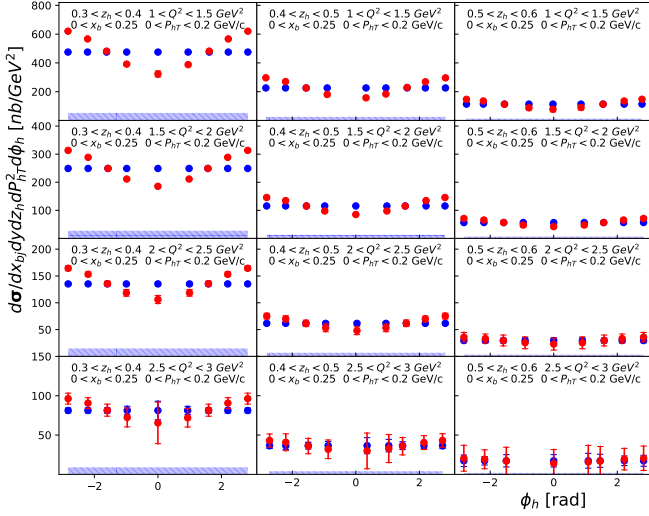


FIG. B1. Unpolarized cross section for π^+ production at 11 GeV in selected kinematic bins: $x_{bj} = [0, 0.25]$, $P_{hT} = [0, 0.2]$ GeV/c, $z_h = [0.3, 0.6]$, $Q^2 = [1, 3]$ GeV². The blue point pseudo-data depict the cross section without the azimuthal modulations, and the cross section with the azimuthal modulations are the red points. The bottom band in each plot describes the total systematic uncertainty from Table I, applied to the blue points only.

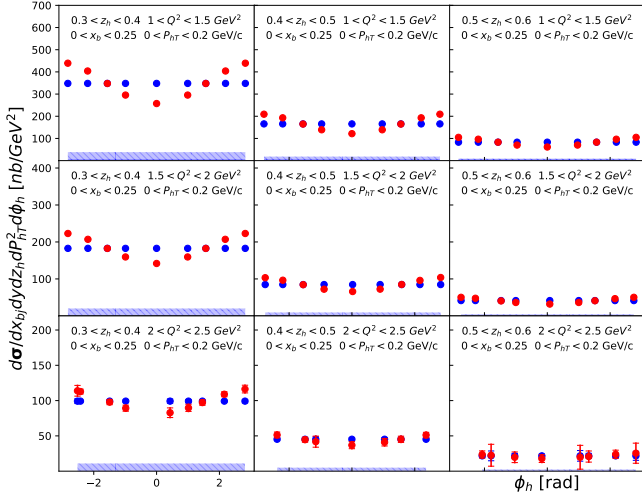


FIG. B2. Unpolarized cross section for π^+ production at 8.8 GeV in selected kinematic bins: $x_{bj} = [0, 0.25]$, $P_{hT} = [0, 0.2]$ GeV/c, $z_h = [0.3, 0.6]$, $Q^2 = [1, 2.5]$ GeV². The rest of the explanation is the same as in Fig. B1.

ures, the systematic and statistical uncertainties are the SoLID statistical uncertainties. All details are given in the figure captions.

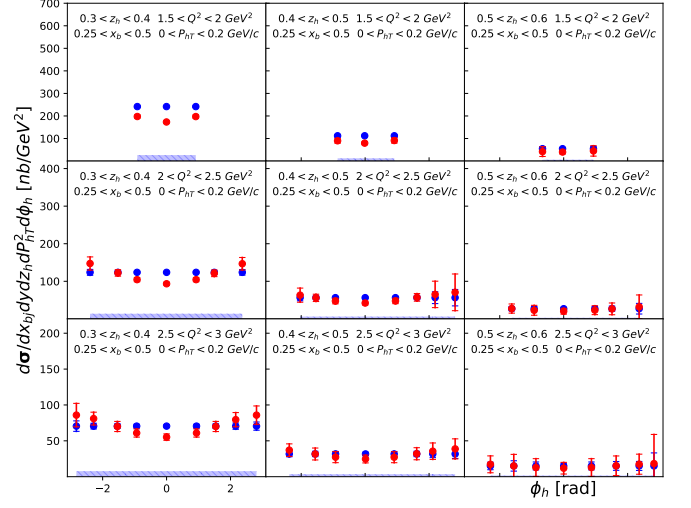


FIG. B3. Unpolarized cross section for π^+ production at 11 GeV in selected kinematic bins: $x_{bj} = [0.25, 0.5]$, $P_{hT} = [0, 0.2]$ GeV/c, $z_h = [0.3, 0.6]$, $Q^2 = [1.5, 3]$ GeV². The rest of the explanation is the same as in Fig. B1.

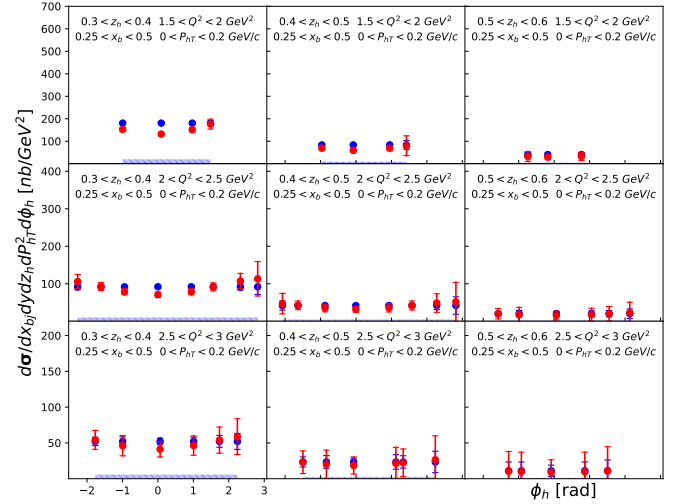


FIG. B4. Unpolarized cross section for π^+ production at 8.8 GeV in selected kinematic bins: $x_{bj} = [0.25, 0.5]$, $P_{hT} = [0, 0.2]$ GeV/c, $z_h = [0.3, 0.6]$, $Q^2 = [1.5, 3]$ GeV². The rest of the explanation is the same as in Fig. B1.

Azimuthal-angle projections of the SoLID SIDIS unpolarized cross section at high- Q^2 region from the general ansatz of Sec. II C

One example at high Q^2 is in turn shown in Fig. B5. Similarly, the bottom band in each plot describes the total systematic uncertainty from Table I, applied to the blue points only.

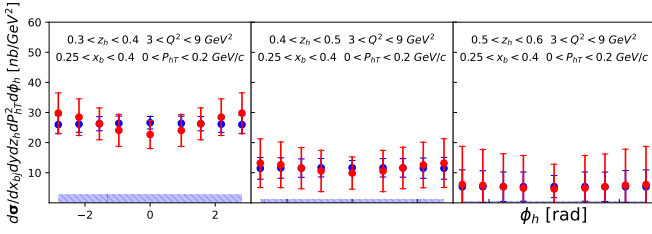


FIG. B5. Unpolarized cross section for π^+ production at 11 GeV in selected kinematic bins: $x_{bj} = [0.25, 0.4]$, $P_{hT} = [0, 0.2]$ GeV/c, $z_h = [0.3, 0.6]$, $Q^2 = [3, 9]$ GeV 2 .

Appendix C: Additional MAP results for Sec. IV C

Here we present the impact study results for the TMD PDFs, Eq. (46), by considering pion and kaon production

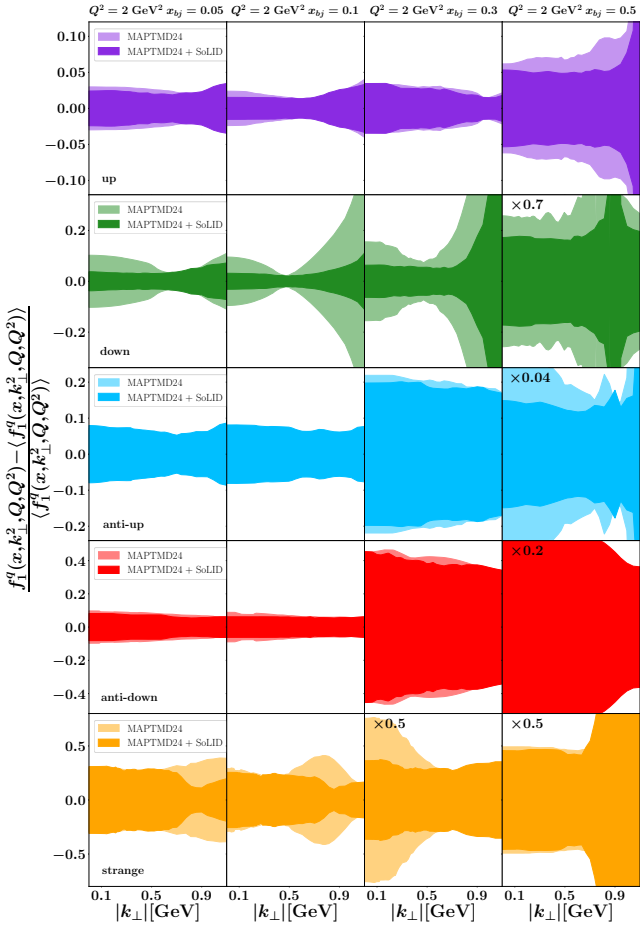


FIG. C1. The MAPTMD24 and impact MAPTMD24+SoLID results on unpolarized TMDs for final-state pions in the bins of $x_{bj} = 0.05$, $x_{bj} = 0.1$, $x_{bj} = 0.3$, $x_{bj} = 0.5$ at $Q^2 = 2$ GeV 2 as a function of $|\mathbf{k}_\perp|$.

separately, still at fixed $Q^2 = 2$ GeV 2 , for different values of $x_{bj} = 0.05, 0.1, 0.3$ and 0.5 , as a function of $|\mathbf{k}_\perp|$.

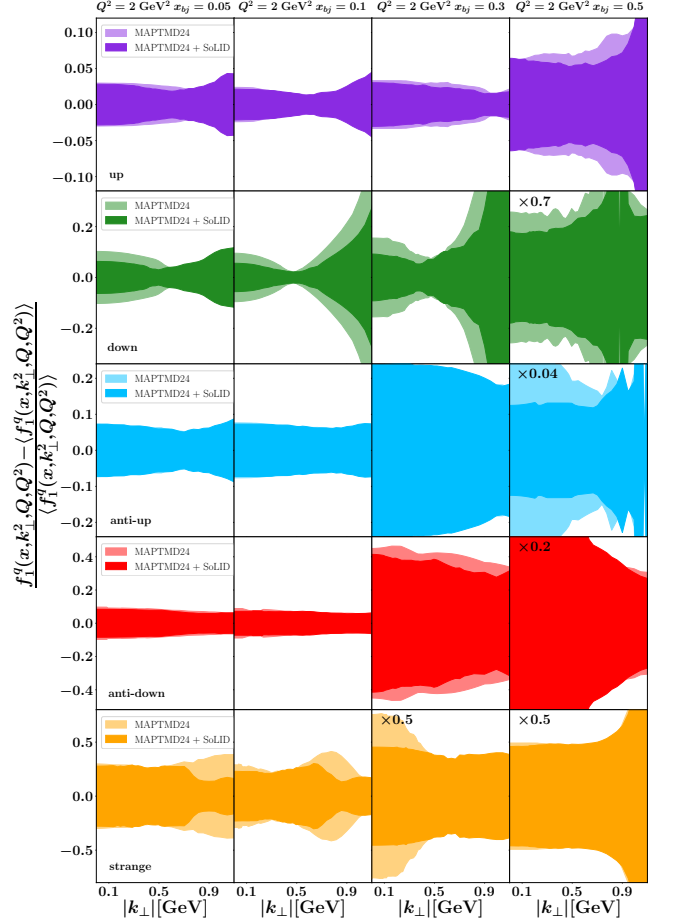


FIG. C2. The MAPTMD24 and impact MAPTMD24+SoLID results on unpolarized TMDs for final-state kaons in the bins of $x_{bj} = 0.05$, $x_{bj} = 0.1$, $x_{bj} = 0.3$, $x_{bj} = 0.5$ at $Q^2 = 2$ GeV 2 as a function of $|\mathbf{k}_\perp|$.

[1] J. J. Ethier and E. R. Nocera, Ann. Rev. Nucl. Part. Sci. **70**, 43-76 (2020) [arXiv:2001.07722 [hep-ph]].

[2] A. Metz and A. Vossen, Prog. Part. Nucl. Phys. **91**, 136-202 (2016) [arXiv:1607.02521 [hep-ex]].

- [3] A. Accardi and J. W. Qiu, *JHEP* **07**, 090 (2008) [arXiv:0805.1496 [hep-ph]].
- [4] R. D. Ball, A. Candido, S. Forte, F. Hekhorn, E. R. Nocera, J. Rojo and C. Schwan, *Eur. Phys. J. C* **82**, no.12, 1160 (2022) [arXiv:2209.08115 [hep-ph]].
- [5] S. Bailey, T. Cridge, L. A. Harland-Lang, A. D. Martin and R. S. Thorne, *Eur. Phys. J. C* **81**, no.4, 341 (2021) [arXiv:2012.04684 [hep-ph]].
- [6] T. J. Hou, J. Gao, T. J. Hobbs, K. Xie, S. Dulat, M. Guzzi, J. Huston, P. Nadolsky, J. Pumplin and C. Schmidt, *et al.* *Phys. Rev. D* **103**, no.1, 014013 (2021) [arXiv:1912.10053 [hep-ph]].
- [7] M. Boglione, A. Dotson, L. Gamberg, S. Gordon, J. O. Gonzalez-Hernandez, A. Prokudin, T. C. Rogers and N. Sato, *JHEP* **10**, 122 (2019) [arXiv:1904.12882 [hep-ph]].
- [8] J. C. Collins and D. E. Soper, *Nucl. Phys. B* **193** (1981), 381 [erratum: *Nucl. Phys. B* **213** (1983), 545] doi:10.1016/0550-3213(81)90339-4
- [9] D. Boer and P. J. Mulders, *Phys. Rev. D* **57**, 5780-5786 (1998) [arXiv:hep-ph/9711485 [hep-ph]].
- [10] R. Boussarie, M. Burkardt, M. Constantinou, W. Detmold, M. Ebert, M. Engelhardt, S. Fleming, L. Gamberg, X. Ji and Z. B. Kang, *et al.* [arXiv:2304.03302 [hep-ph]].
- [11] K. Goeke, A. Metz and M. Schlegel, *Phys. Lett. B* **618**, 90-96 (2005) [arXiv:hep-ph/0504130 [hep-ph]].
- [12] A. Bacchetta, M. Diehl, K. Goeke, A. Metz, P. J. Mulders and M. Schlegel, *JHEP* **02**, 093 (2007) [arXiv:hep-ph/0611265 [hep-ph]].
- [13] S. M. Aybat and T. C. Rogers, *Phys. Rev. D* **83**, 114042 (2011) [arXiv:1101.5057 [hep-ph]].
- [14] R. Angeles-Martinez, A. Bacchetta, I. I. Balitsky, D. Boer, M. Boglione, R. Boussarie, F. A. Ceccopieri, I. O. Cherednikov, P. Connor and M. G. Echevarria, *et al.* *Acta Phys. Polon. B* **46**, no.12, 2501-2534 (2015) [arXiv:1507.05267 [hep-ph]].
- [15] V. Barone, M. Boglione, J. O. Gonzalez Hernandez and S. Melis, *Phys. Rev. D* **91**, no.7, 074019 (2015) [arXiv:1502.04214 [hep-ph]].
- [16] M. Anselmino, M. Boglione, U. D'Alesio, S. Melis, F. Murgia, E. R. Nocera and A. Prokudin, *Phys. Rev. D* **83**, 114019 (2011) [arXiv:1101.1011 [hep-ph]].
- [17] S. Bastami, H. Avakian, A. V. Efremov, A. Kotzinian, B. U. Musch, B. Parsamyan, A. Prokudin, M. Schlegel, G. Schnell and P. Schweitzer, *et al.*, *JHEP* **06**, 007 (2019) [arXiv:1807.10606 [hep-ph]].
- [18] A. Bacchetta, *AIP Conf. Proc.* **1149**, no.1, 447-452 (2009) doi:10.1063/1.3215686 [arXiv:0902.2712 [hep-ph]].
- [19] A. Airapetian, *et al.* [HERMES], *Nucl. Instrum. Meth. A* **540**, 68-101 (2005) [arXiv:physics/0408137 [physics.ins-det]].
- [20] S. Goertz, W. Meyer and G. Reicherz, *Prog. Part. Nucl. Phys.* **49**, 403-489 (2002) [erratum: *Prog. Part. Nucl. Phys.* **51**, 309-312 (2003)].
- [21] X. Qian *et al.* [Jefferson Lab Hall A], *Phys. Rev. Lett.* **107**, 072003 (2011) [arXiv:1106.0363 [nucl-ex]].
- [22] J. Huang *et al.* [Jefferson Lab Hall A], *Phys. Rev. Lett.* **108**, 052001 (2012) [arXiv:1108.0489 [nucl-ex]].
- [23] D. Boer and W. Vogelsang, *Phys. Rev. D* **74**, 014004 (2006) doi:10.1103/PhysRevD.74.014004 [arXiv:hep-ph/0604177 [hep-ph]].
- [24] S. Arnold, A. Metz and M. Schlegel, *Phys. Rev. D* **79**, 034005 (2009) [arXiv:0809.2262 [hep-ph]].
- [25] J. C. Collins, D. E. Soper and G. F. Sterman, *Nucl. Phys. B* **250** (1985), 199-224 doi:10.1016/0550-3213(85)90479-1
- [26] A. Bacchetta, M. G. Echevarria, P. J. G. Mulders, M. Radici and A. Signori, *JHEP* **11**, 076 (2015) doi:10.1007/JHEP11(2015)076 [arXiv:1508.00402 [hep-ph]].
- [27] J. Arrington *et al.* [Jefferson Lab SoLID], The Solenoidal Large Intensity Device (SoLID) for JLab 12 GeV, *J. Phys. G: Nucl. Part. Phys.* **50** 110501 (2023).
- [28] [SoLID], SoLID (Solenoidal Large Intensity Device) Updated Preliminary Conceptual Design Report, <https://solid.jlab.org/DocDB/0002/000282/001/solid-precdr-2019Nov.pdf>
- [29] J. P. Chen *et al.* [SoLID], A White Paper on SoLID (Solenoidal Large Intensity Device), [arXiv:1409.7741 [nucl-ex]].
- [30] J. Dudek, R. Ent, R. Essig, K. S. Kumar, C. Meyer, R. D. McKeown, Z. E. Meziani, G. A. Miller, M. Pennington and D. Richards, *et al.* *Eur. Phys. J. A* **48** (2012), 187 [arXiv:1208.1244 [hep-ex]].
- [31] J. Arrington *et al.*, *Progress in Particle and Nuclear Physics*, **127**, 103985 (2022).
- [32] Jefferson Lab Experiment E12-10-006, Spokespersons: J.-P. Chen, H. Gao (contact), X. D. Jiang, J. C. Peng and A. Qian, Target Single Spin Asymmetry in Semi-Inclusive Deep-Inelastic ($e, e'\pi^\pm$) Reaction on a Transversely Polarized ^3He Target at 11 GeV, <https://solid.jlab.org/experiments.html>
- [33] H. Gao, L. Gamberg, J. P. Chen, X. Qian, Y. Qiang, M. Huang, A. Afanasev, M. Anselmino, H. Avakian and G. Cates, *et al.* *Eur. Phys. J. Plus* **126**, 2 (2011) [arXiv:1009.3803 [hep-ph]].
- [34] Jefferson Lab Experiment E12-11-007, Spokespersons: J.-P. Chen, J. Huang (contact), C. Peng, Y. Qiang and W. B. Yan, Asymmetries in Semi-Inclusive Deep-Inelastic ($e, e'\pi^\pm$) Reactions on a Longitudinally Polarized ^3He Target at 8.8 and 11 GeV, <https://solid.jlab.org/experiments.html>
- [35] Jefferson Lab Experiment E12-11-108, Spokespersons: K. Allada, J.-P. Chen, H. Gao (contact), V. Khachatryan, X. M. Li and Z.-E. Meziani, Target Single Spin Asymmetry in Semi-Inclusive Deep-Inelastic ($e, e'\pi^\pm$) Reaction on a Transversely Polarized Proton Target, <https://solid.jlab.org/experiments.html>
- [36] I. Scimemi and A. Vladimirov, *JHEP* **06**, 137 (2020) doi:10.1007/JHEP06(2020)137 [arXiv:1912.06532 [hep-ph]].
- [37] A. Bacchetta *et al.* [MAP (Multi-dimensional Analyses of Partonic distributions)], *JHEP* **10**, 127 (2022) doi:10.1007/JHEP10(2022)127 [arXiv:2206.07598 [hep-ph]].
- [38] A. Bacchetta *et al.* [MAP (Multi-dimensional Analyses of Partonic distributions)], *JHEP* **08**, 232 (2024) [arXiv:2405.13833 [hep-ph]].
- [39] V. H. Moos, I. Scimemi, A. Vladimirov and P. Zurita, *JHEP* **11**, 134 (2025) doi:10.1007/JHEP11(2025)134 [arXiv:2503.11201 [hep-ph]].
- [40] A. Airapetian *et al.* [HERMES], *Phys. Rev. D* **87**, 074029 (2013) [arXiv:1212.5407 [hep-ex]].
- [41] M. Aghasyan, *et al.* [COMPASS], *Phys. Rev. D* **97**, no.3, 032006 (2018) [arXiv:1709.07374 [hep-ex]].
- [42] M. Osipenko, *et al.* [CLAS], *Phys. Rev. D* **80**, 032004 (2009) [arXiv:0809.1153 [hep-ex]].

- [43] J. Osvaldo Gonzalez-Hernandez, PoS **DIS2019**, 176 (2019).
- [44] M. Alrashed, Z. B. Kang, J. Terry, H. Xing and C. Zhang, “Nuclear modified transverse momentum dependent parton distribution and fragmentation functions,” [arXiv:2312.09226 [hep-ph]].
- [45] M. Cerutti, A. Accardi, I. P. Fernando, S. Li, J. F. Owens and S. Park, Phys. Rev. D **111**, no.9, 9 (2025) [arXiv:2501.06849 [hep-ph]].
- [46] A. Martin, Int. J. Mod. Phys. Conf. Ser. **40**, 1660028 (2016).
- [47] R. Asaturyan, R. Ent, H. Mkrtchyan, T. Navasardyan, V. Tadevosyan, G. S. Adams, A. Ahmidouch, T. Angelescu, J. Arrington and A. Asaturyan, *et al.* [Jefferson Lab Hall C], Phys. Rev. C **85**, 015202 (2012) [arXiv:1103.1649 [nucl-ex]].
- [48] T. Navasardyan, G. S. Adams, A. Ahmidouch, T. Angelescu, J. Arrington, R. Asaturyan, O. K. Baker, N. Benmouna, C. Bertonecini and H. P. Blok, *et al.* Phys. Rev. Lett. **98**, 022001 (2007) [arXiv:hep-ph/0608214 [hep-ph]].
- [49] X. Yan, *et al.* [Jefferson Lab Hall A], Phys. Rev. C **95**, no.3, 035209 (2017) [arXiv:1610.02350 [nucl-ex]].
- [50] X. Yan, Unpolarized SIDIS Cross Section from a ^3He Target, PhD Thesis, Duke University (2017), <https://www.osti.gov/biblio/1419164>
- [51] Jefferson Lab Experiment E12-09-017, Spokespersons: P. Bosted, R. Ent, H. Mkrtchyan, Transverse Momentum Dependence of Semi-Inclusive Pion and Kaon Production, https://www.jlab.org/exp_prog/PACpage/PAC38/proposals/Previously_Approved/E12-09-017_Update.pdf
- [52] M. Anselmino, M. Boglione, J. O. Gonzalez Hernandez, S. Melis and A. Prokudin, JHEP **04**, 005 (2014) [arXiv:1312.6261 [hep-ph]].
- [53] A. Bacchetta and M. Radici, Phys. Rev. Lett. **107**, 212001 (2011) [arXiv:1107.5755 [hep-ph]].
- [54] M. Anselmino, M. Boglione, U. D’Alesio, A. Kotzinian, F. Murgia and A. Prokudin, Phys. Rev. D **71**, 074006 (2005) [arXiv:hep-ph/0501196 [hep-ph]].
- [55] A. Bacchetta, G. Bozzi, M. G. Echevarria, C. Pisano, A. Prokudin and M. Radici, Phys. Lett. B **797** (2019), 134850 [arXiv:1906.07037 [hep-ph]].
- [56] A. Vladimirov, V. Moos and I. Scimemi, JHEP **01** (2022), 110 [arXiv:2109.09771 [hep-ph]].
- [57] M. A. Ebert, A. Gao and I. W. Stewart, JHEP **06** (2022), 007 [erratum: JHEP **07** (2023), 096] [arXiv:2112.07680 [hep-ph]].
- [58] S. Rodini and A. Vladimirov, Phys. Rev. D **110** (2024) no.3, 034009 [arXiv:2306.09495 [hep-ph]].
- [59] L. Gamberg, Z. B. Kang, D. Y. Shao, J. Terry and F. Zhao, [arXiv:2211.13209 [hep-ph]].
- [60] T. Liu, Z. Zhao, W. Xiong, H. Gao, LiuSIDIS: A sidis event generator, <https://github.com/Tianboliu/LiuSIDIS>
- [61] Jefferson Lab Run-group Experiment with E12-10-006 and E12-11-007, Spokespersons: M. Cerutti, U. D’alesio, H. Gao (contact), S. Jia, V. Khachatryan and Y. Tian, Measurement of the Unpolarized SIDIS Cross Section from a ^3He Target with SoLID, https://webhome.phy.duke.edu/~mep/SoLID_unpol_xs_proposal.pdf
- [62] A. Bacchetta, U. D’Alesio, M. Diehl and C. A. Miller, Phys. Rev. D **70**, 117504 (2004) [arXiv:hep-ph/0410050 [hep-ph]].
- [63] D. Byer, V. Khachatryan, H. Gao, I. Akushevich, A. Ilyichev, C. Peng, A. Prokudin, S. Srednyak and Z. Zhao, Comput. Phys. Commun. **287**, 108702 (2023) [arXiv:2210.03785 [hep-ph]].
- [64] J. C. Collins and D. E. Soper, Nucl. Phys. B **197**, 446-476 (1982).
- [65] J. Collins, “Foundations of Perturbative QCD”, Cambridge University Press, (2013).
- [66] A. Bacchetta, R. Kundu, A. Metz and P. J. Mulders, Phys. Lett. B **506**, 155-160 (2001) [arXiv:hep-ph/0102278 [hep-ph]].
- [67] P. Schweitzer, T. Teckentrup and A. Metz, Phys. Rev. D **81**, 094019 (2010) [arXiv:1003.2190 [hep-ph]].
- [68] A. Accardi, L. T. Brady, W. Melnitchouk, J. F. Owens and N. Sato, Phys. Rev. D **93**, no.11, 114017 (2016) [arXiv:1602.03154 [hep-ph]].
- [69] D. de Florian, R. Sassot and M. Stratmann, Phys. Rev. D **75**, 114010 (2007) [arXiv:hep-ph/0703242 [hep-ph]].
- [70] V. Barone, S. Melis and A. Prokudin, Phys. Rev. D **81**, 114026 (2010) [arXiv:0912.5194 [hep-ph]].
- [71] M. Anselmino, M. Boglione, U. D’Alesio, S. Melis, F. Murgia and A. Prokudin, Phys. Rev. D **87**, 094019 (2013) [arXiv:1303.3822 [hep-ph]].
- [72] T. Liu, Private communication.
- [73] E. Christova, D. Kotlorz and E. Leader, Phys. Rev. D **102**, no.1, 014035 (2020) [arXiv:2004.02117 [hep-ph]].
- [74] S. Scopetta, Phys. Rev. D **104**, 054005, (2007).
- [75] J. J. Aubert *et al.* [European Muon], Phys. Lett. B **123**, 275-278 (1983).
- [76] R. G. Arnold, P. E. Bosted, C. C. Chang, J. Gomez, A. T. Katramatou, G. Petratos, A. A. Rahbar, S. Rock, A. F. Sill and Z. M. Szalata, *et al.* Phys. Rev. Lett. **52**, 727 (1984).
- [77] D. Abrams *et al.* [Jefferson Lab Hall A Tritium], Phys. Rev. Lett. **135**, no.6, 062502 (2025) [arXiv:2410.12099 [nucl-ex]].
- [78] A. Bacchetta *et al.* [MAP (Multi-dimensional Analyses of Partonic distributions)], JHEP **10**, 127 (2022) [arXiv:2206.07598 [hep-ph]].
- [79] D. Boer, L. Gamberg, B. Musch and A. Prokudin, JHEP **10**, 021 (2011) [arXiv:1107.5294 [hep-ph]].
- [80] D. Boer, Few Body Syst. **56**, no.6-9, 439-445 (2015) [arXiv:1409.8317 [hep-ph]].
- [81] O. del Rio, A. Prokudin, I. Scimemi and A. Vladimirov, Phys. Rev. D **110** (2024) no.1, 1 [arXiv:2402.01836 [hep-ph]].
- [82] E. Moffat *et al.* [Jefferson Lab Angular Momentum (JAM)], Phys. Rev. D **104**, no.1, 016015 (2021) [arXiv:2101.04664 [hep-ph]].
- [83] M. Murphy, H. Dai, L. Gu, D. Abrams, A. M. Ankowski, B. Aljawrneh, S. Alsalmi, J. Bane, S. Barcus and O. Benhar, *et al.* [The Jefferson Lab Hall A Collaboration], Phys. Rev. C **100**, no.5, 054606 (2019). [arXiv:1908.01802 [hep-ex]].
- [84] R. D. Ball *et al.* [NNPDF], Eur. Phys. J. C **77**, no.10, 663 (2017) [arXiv:1706.00428 [hep-ph]].
- [85] A. Del Dotto, L. P. Kaptari, E. Pace, G. Salmè and S. Scopetta, Phys. Rev. C, **96**, 065203 (2017).
- [86] Á. Kripkó and S. Diehl, Extraction of the $\cos\phi$ and $\cos2\phi$ cross-section moments of charged kaon SIDIS, https://indico.jlab.org/event/928/contributions/16228/attachments/12264/19427/Kripko_kaon_sidis_cos.pdf